Available online at www.sciencedirect.com
SCIENCE DIRECT
Precambrian Research 145 (2006) 159–181
Precambrian Research
www.elsevier.com/locate/precamres

Granulite xenoliths and their zircons, Tuoyun, NW China: Insights into southwestern Tianshan lower crust

Jianping Zheng [a,b,*], W.L. Griffin [b,c], Suzanne Y. O'Reilly [b], Ming Zhang [b], J.G. Liou [d], Norman Pearson [b]

[a] State Key Laboratory of Geological Processes and Mineral Resources, China University of Geosciences, Wuhan 430074, China
[b] GEMOC ARC National Key Center, Department of Earth and Planetary Sciences, Macquarie University, NSW 2109, Australia
[c] CSIRO Exploration and Mining, North Ryde, NSW 2113, Australia
[d] Department of Geological and Environmental Sciences, Stanford University, CA 94305, USA

Received 26 May 2005; received in revised form 21 November 2005; accepted 2 December 2005

Abstract

Granulite xenoliths from the Cretaceous-Paleogene Tuoyun basalts in the southwestern Tianshan area (NW China) are mainly pyroxene granulite and olivine granulite, with minor garnet granulite and quartz granulite. They can be divided into two types by geochemistry and petrography; both are interpreted as magmatic rocks that have undergone multistage metamorphism. Type I granulites are foliated, mafic to intermediate in composition and have negative Zr and Hf anomalies. Type II xenoliths are massive mafic rocks with high Ni contents, and little or no Zr and Hf anomaly. *P–T* estimates for garnet granulites suggest the xenoliths were derived from depths of ca. 40 km, near the base of the crust. LAM-ICPMS U–Pb data for zircons from four xenoliths lie on discordia with upper intercepts of 690–770 Ma and lower intercepts of 80–125 Ma. Oscillatory zoning in zircon cores suggests that the upper-intercept ages reflect magmatic crystallization and subsequent granulite-facies metamorphism, and the lower intercepts reflect a major thermal event in the lower crust, related to the eruption of the host basalts. Hf-isotope compositions show little variation with age, indicating that most zircons with young ages were thermally reset. Mean Hf model ages for the zircons from each xenolith range from 1.3 to 1.7 Ga. These data and whole-rock chemistry suggest that the protoliths of the granulites were generated by underplating of mafic magmas that assimilated variable proportions of pre-existing crust. Simple modeling of the Hf-isotope data indicates that this lower crust contained components ≥2.5 Ga, and probably >3.4 Ga, in age in Neoproterozoic time. These observations suggest that the southwestern Tianshan (e.g. in Tuoyun area) may represent the presence of a microcontinental block within the Paleozoic East Central Asian Orogenic Belt.

Keywords: Granulite xenoliths; Geochemistry; Geochronology; Hf-isotope; Zircon; Lower crust; Southwestern Tianshan; Northwest China

1. Introduction

The continental crust grows both by horizontal accretion at the plate boundaries and vertical accretion within the plates (Griffin and O'Reilly, 1986; Condie, 1999). The mountains of the Tianshan (Tien Shan) range extend east–west for at least 2500 km across central Asia, from Uzbekistan, Tajikistan and Kirghizia to northwestern China, and are part of the larger Indian–Asian collision system. Studies on the Tianshan and adjacent regions have mainly concentrated on the Paleozoic collision tectonics and their evolution (e.g. Coleman, 1989; Windley et al., 1990; Allen et al., 1992; Shi et al., 1994; Gao et al., 1998; Chen et al., 1999; Gao and Klemd,

* Corresponding author.
E-mail address: jpzheng@cug.edu.cn (J. Zheng).

0301-9268/$ – see front matter © 2005 Elsevier B.V. All rights reserved.
doi:10.1016/j.precamres.2005.12.001

2003), Mesozoic-Cenozoic intra-continent basin evolution (Carroll et al., 1995; Graham et al., 1990; Allen et al., 1991; Hendrix et al., 1994) and neotectonics (Nelson et al., 1987; Fu, 2000; Chen et al., 2002). It is broadly accepted that the Tianshan is a complex Paleozoic orogen with composite terrains (e.g. Windley et al., 1990; Xiao et al., 1992; Hu et al., 2000). Uplift began with accompanying volcanic eruptions and the intrusion of granites in early Permian time. The uplift accelerated in the late Permian and continental molasse was extensively deposited. Since the late Permian the Tianshan has been magmatically quiescent except for the eruption of a small volume of basaltic rocks (Sobel and Arnaud, 2000). These basalts contain abundant megacrysts (amphibole, pyroxene and anorthoclase) and deep-seated xenoliths of both upper-mantle and lower-crust lithologies (Han et al., 1998; Zheng et al., 2001). Studies of the peridotite xenoliths have shown that the Tianshan mantle consists largely of fertile lherzolites with relics of more depleted, possibly Proterozoic mantle (Zheng et al., 2005).

Based on the low Sm–Nd ages of minerals and whole-rock samples of granulite xenoliths in the Tariat and the Dariganga alkali basalts of the East Central Asia Phanerozoic Orogenic Belt (Fig. 1A), Stosch et al. (1995) suggested that the lower crust beneath the orogenic belt may be young (Cenozoic) or that ambient temperatures in the lower crust were high enough to permit continuous isotopic equilibration. Lower crustal xenoliths from the Cretaceous-Paleogene Tuoyun basaltic rocks include pyroxene granulite, olivine granulite, garnet granulite and quartz granulite. The age and petrogenesis of these granulites are significant for understanding the nature of the lower crust beneath the Tianshan. Geochemical data on the granulite xenoliths, and U–Pb and Hf-isotope analyses of their zircons, are presented here to discuss the formation and evolution of the southwestern Tianshan lower crust.

2. Geological setting and petrography

The Tianshan is one of the most important Paleozoic orogenic belts in central Asia. In NW China, the Tianshan Mountains lie in the Xinjiang region between the Junggar terrane to the north and the Tarim block to the south (Fig. 1B). The basement of the Junggar terrane is interpreted as a juvenile crust, dominated by early Paleozoic oceanic crust and arc complexes that were deeply buried during the late Paleozoic subduction and accretion (Chen and Jahn, 2004). The Tarim block is separated from the Yili-Central Tianshan block by the Southern Central Tianshan suture (Early Carboniferous). Ophiolitic mélanges and blueschists are widespread in this suture and are believed to be produced by collision between a passive continental margin on the north side of the Tarim plate and an active continental margin on the south side of the Yili-Central Tianshan plate at the end of Early Carboniferous (Gao et al., 1998). The Archean bimodal suite (TTG gneisses and amphibolites) and Proterozoic granitic gneisses with Nd model ages of 3.2–2.2 Ga are found in the northeastern Tarim block (Hu et al., 2000), and Neoproterozoic blueschists and greenschists are exposed in the northwestern part of the block (689–719 Ma; Nakajima, 1990; Xiao et al., 1992), adjacent to the southern Tianshan region.

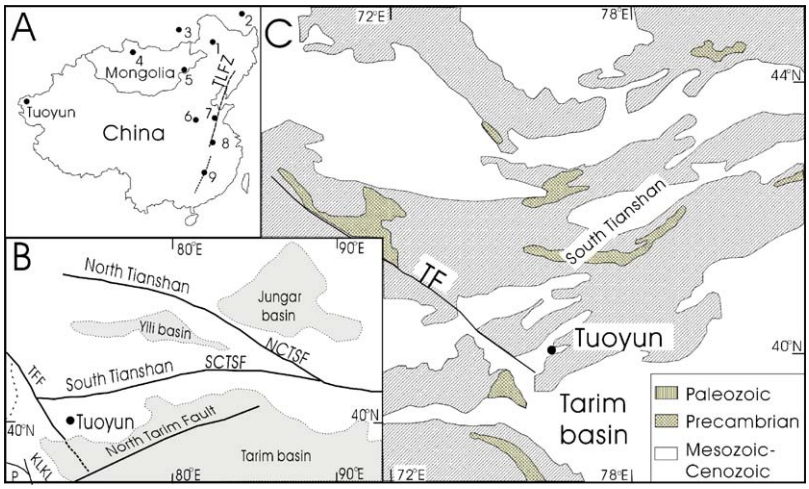

Fig. 1. Locality of the Tuoyun xenoliths and geological sketch map of South Tianshan. (1) Tariat, (2) Dariganga, (TFF) Talas-Ferghana strike-slip fault; (P) Pamir, (KLKL) Karakunlunshan, (SCTSF) Southern Central-Tianshan Fault, (NCTSF) Northern Central-Tianshan Fault. Modified after Allen et al. (1992) and Brookfield (2000).

The Tianshan formed by accretion of Phanerozoic subduction complexes (e.g. Gao et al., 1995, 1998; Gao and Klemd, 2003) with entrained Proterozoic basement rocks recorded by Nd model ages of exposed amphibolite and granitic gneisses (2.2–1.2 Ga with peak at 2.1–1.7 Ga; Hu et al., 1997, 2000) and zircon U–Pb ages on granitic-tonalitic-granodioritic gneiss (882–707 Ma; Chen, 1999; Chen et al., 2000). The Tianshan splits into northern and southern branches separated by the Yili microcontinent, and can be subdivided into three portions along its length: the eastern section is located in Chinese territory east of the lake Issyk Kul; the central section extents west to the Talas-Ferghana (TF) strike-slip fault; the western section extents west from this fault (Fig. 1A).

The Tuoyun basin is located in the southern Tianshan area, adjacent to the northern part of the Tarim basin, east of the Talas-Ferghana strike-slip fault (TFF). It preserves a volumetrically small series of basalt flows ca. 25 m thick, interbedded with Mesozoic-Paleogene sedimentary rocks (Fig. 1C). The flows have yielded whole-rock $^{40}Ar/^{39}Ar$ ages of 120–110 and 67–46 Ma (Sobel and Arnaud, 2000). A zircon SHRIMP U–Pb age of 48.1 ± 1.6 Ma was recently reported from the basaltic flows (Liang et al., 2005).

The granulite xenoliths used in this study were collected from the lower part of the basalts, at a location 1 km south of the Tuoyun County (40°9.50′N and 75°20.54′E), NW China. They are accompanied by abundant peridotite and pyroxenite xenoliths, and megacrysts (up to 9 cm long) of amphibole, pyroxene and anorthoclase. The granulite xenoliths are 8–18 cm in diameter and fresh. Thirteen thin sections from the Tuoyun granulite xenoliths were examined. Mineral assemblages and their modes, determined by point-counting more than 1500 points in each thin section, are listed in Table 1.

Orthopyroxene + clinopyroxene + plagioclase ± K-feldspar is the typical assemblage of metamorphic minerals. The xenoliths are medium- to fine-grained (1–3 mm) and have well-developed granoblastic fabrics (mostly polygonal). Two types of structures are recognized: (1) banded structure (Type I), defined by alternating pyroxene-rich and plagioclase-rich layers, and (2) massive structure (Type II). The former contains higher plagioclase modes (43.6–58.6 vol%) than the latter (35.3–42.2 vol%). Type I xenoliths include major pyroxene granulite, and minor garnet granulite (TY15 and TY65) and quartz granulite (TY1b and TY7d). Type II xenoliths are mainly olivine granulite and minor pyroxene granulite. Some samples preserve relict magmatic orthopyroxene or clinopyroxene, showing evidence of multistage metamorphism. Relict orthopyroxenes in TY62 (Type I) and in TY12 (Type II) are surrounded by polygonal aggregates of clinopyroxene + plagioclase + ilmenite, whereas relict clinopyroxenes in TY16 (Type II) are rimmed by polygonal aggregates of orthopyroxene + plagioclase + ilmenite. Ilmenite with hematite lamellae is the most common accessory mineral. Minor biotite and apatite occur in some Tuoyun granulites (see Table 1).

3. Analytical methods

Zircons were separated from four xenoliths using standard heavy mineral techniques, and were mounted

Table 1
Modal compositions of Tuoyun granulite xenoliths (%)

Type	Sample	Rock type	Structure	Cpx	Opx	Pl	Grt	Ol	Kfs	Qtz	Bt	Ilm	Ap
Type I	TY13	Pyroxene granulite	Foliated	18.2	22.7	52.0			2.1		1.9	3.1	
	TY62	Pyroxene granulite	Foliated	27.2	23.3	43.6					0.7	5.2	
	TY67	Pyroxene granulite	Foliated	26.1	25.4	43.6			1.6			3.3	
	TY1b	Quartz granulite	Foliated	20.2	18.5	53.9				5.2	0.9	1.3	
	TY7d	Quartz granulite	Foliated	19.3	17.0	57.1			1.5	3.8	0.3	1.0	
	TY15	Garnet granulite	Foliated	23.7	21.2	47.1	8.0						
	TY65	Garnet granulite	Foliated	24.4	20.9	47.8	6.9						
Type II	TY16	Pyroxene granulite	Massive	27.4	27.6	42.2						2.8	
	TY17	Pyroxene granulite	Massive	27.0	27.2	41.9						3.9	
	TY61	Pyroxene granulite	Massive	24.1	27.5	40.1			2.2		1.8	2.1	2.2
	TY12	Olivine granulite	Massive	24.1	27.2	37.4		4.9	0.5		1.7	4.2	
	T4p3	Olivine granulite	Massive	26.3	33.9	35.3		2.1				2.4	
	T5ap2	Olivine granulite	Massive	28.1	29.3	37.9		1.6				3.1	
	T7dp2	Olivine granulite	Massive	28.3	27.6	38.8		3.4				1.9	

Mineral modes were determined by point-counting more than 1500 points in each thin section.

in epoxy blocks for analysis. Images of each zircon were made with a combination of cathodoluminescence and electron backscattering (BSE/CL), using a Cameca SX-50 Electron Microprobe operating at 15 kV and 20 nA, at the GEMOC Key Centre, Macquarie University. These images have been used to identify different stages of zircon growth, to distinguish igneous from recrystallised or metamorphic zircons, and to select the positions for LAM-ICPMS and LAM-MC-ICPMS analyses.

3.1. Major element analysis of minerals

Mineral compositions were analyzed using a Cameca SX 50 electron microprobe at GEMOC, fitted with five crystal spectrometers with same accelerating voltage and sample current as for BSE/CL imaging. The width of the electron beam was 5 μm. Standards were natural minerals and matrix corrections were performed employing the PAP method (Pouchou and Pichoir, 1984). Counting times were 10 s for each peak and 5 s for background on both sides of the peak. Major oxide contents of silicate minerals from the Tuoyun granulite xenoliths are presented in Table 2 . Each analysis generally represents the average of five point analyses on an individual grain. In order to examine whether compositional equilibrium was attained, considerable attention was paid to determining the homogeneity of individual phases between core and rim. The results indicate that the granoblastic minerals of all the Tuoyun granulite xenoliths are homogeneous within analytical precision. Contents of Fe^{3+} in pyroxenes and garnet were calculated from mineral stoichiometry. For zircon analyses, the spatial resolution of the electron microprobe was about 2 μm. Lower limits of detection were 0.1% for Hf, and ca. 0.03% for Y, Th and U (as the oxides). Representative results are shown in Table 3.

3.2. Chemical analyses of whole rocks

Eleven granulite xenoliths were analyzed for major and trace elements. After removal of outer portions, the samples were crushed in a hardened jaw crusher, and then powdered in an agate mill down to a grain size smaller than 200 mesh. Chemical analysis was carried out at China University of Geosciences (Wuhan). Major element oxides were determined by wet chemical analysis (Table 4). For trace element analyses, ca. 50 mg were dissolved in distilled $HF + HNO_3$ (3:1) in Savillex Teflon screw-cap capsules at 100 °C for 2 days, dried and then digested with 6 M HCl at 150 °C. Three duplicates of three standards (AGV-1, GSR-3 and DNC-1) were prepared using the same procedure, to monitor the analytical precision. The solutions were measured for trace elements using a POEMS-III ICP mass spectrometer (MS). The discrepancy among triplicates is less than 10% for all elements (Table 5). Analyses of standards are in agreement with the recommended values. The analytical procedures were after Lin et al. (2000).

3.3. U–Pb dating of zircons

In situ U–Pb isotope analyses of zircons from four samples were carried out at GEMOC. These results are shown in Table 6. Grain mounts containing the samples and the GEMOC GJ1 zircon standard were cleaned in 2N nitric acid for ca. 1 h prior to analysis. LAM-ICPMS analyses were performed using a custom-built 213 nm UV LAM (Norman et al., 1996) coupled to an Agilent HP4500 (series 300) ICPMS. ICPMS operating conditions and data acquisition parameters are given by Belousova et al. (2001) and Jackson et al. (2004). Samples and standard were ablated in He to minimize deposition of ablation products around ablation sites and improve sample transport efficiency; this procedure also gives more stable signals and more reproducible Pb/U fractionation. To minimize dynamic U/Pb fractionation as the laser beam penetrates into the sample (Hirata and Nesbitt, 1995), analyses were performed with the laser focused above the sample (typically ∼200 μm). Identical laser operating conditions were rigorously maintained throughout each run of 20 analyses to ensure constant U/Pb fractionation. Ablation pit diameter was generally about 30–40 μm.

Samples were analyzed in separate 'runs' of 20 analyses comprising 12 analyses of unknowns bracketed by four analyses of the GEMOC GJ1 zircon standard, a gem quality zircon that contains ca. 260 ppm U; multiple thermal ionisation mass spectroscopy (TIMS) analyses show it to be 608.5 ± 0.4 Ma old ($^{207}Pb/^{206}Pb$ age) and slightly discordant. Each analysis was ∼180 s, with gas background measurements being taken over the first ∼60 s, before initiation of ablation. Data were acquired on five masses (206–208, 232, 235) with short dwell times to provide quasi-simultaneous measurement of the five masses and optimum precision. Time-resolved signals (i.e. signals as a function of time, which is a proxy for ablation depth) allow isotopic heterogeneity within the ablation volume to be clearly identified (e.g. zones of Pb loss or common Pb related to fractures or areas of radiation damage; also inclusions, inherited cores, etc.).

Raw data were processed using GLITTER, an on-line data reduction program developed at GEMOC (www.es.mq.edu.au/GEMOC/). $^{207}Pb/^{206}Pb$, $^{208}Pb/^{232}Th$, $^{206}Pb/^{238}U$ and $^{207}Pb/^{235}U$ ($^{235}U = {}^{238}U/137.88$) ratios

Table 2
Representative electron microprobe analyses of minerals from Tuoyun granulite xenoliths (wt%)

	Type I																				
Sample	TY13						TY62							TY67					TY1b		
Rock	Pyroxenes granulite						Pyroxenes granulite							Pyroxenes granulite					Quartz granulite		
Mineral	Cpx	Opx	Pl	Kfs	Ilm	Hem	Cpx	Opx	$Opx_{(I)}$	Pl	Kfs	Ilm	Hem	Cpx	Opx	Pl	Hem	Ilm	Cpx	Opx	Pl
Points	5	5	5	3	5	5	5	5	3	5	3	5	5	5	5	5	5	5	5	5	5
SiO_2	50.8	50.8	56.2	59.1	0.00	0.14	50.5	50.7	51.1	58.3	63.2	0.05	1.57	50.9	51.0	53.6	0.08	0.04	51.0	50.9	57.3
TiO_2	0.28	0.08	0.01	0.52	50.1	20.6	0.32	0.10	0.06	0.01	0.00	49.3	15.3	0.30	0.06	0.02	8.38	44.6	0.23	0.09	0.01
Al_2O_3	3.24	2.07	26.9	22.9	0.03	1.21	3.48	2.17	2.08	25.7	19.7	0.07	2.03	3.44	2.35	28.6	2.50	0.15	2.85	1.72	26.2
Cr_2O_3	0.02	0.01	0.01	0.00	0.04	0.23	0.03	0.00	0.01	0.00	0.01	0.00	0.27	0.01	0.02	0.01	0.23	0.07	0.02	0.03	0.01
FeO	11.3	25.4	0.22	0.74	46.7	72.6	12.4	26.6	26.7	0.41	0.46	47.1	70.1	10.3	24.5	0.29	80.9	48.8	12.3	27.4	0.19
MnO	0.23	0.49	0.02	0.00	0.07	0.38	0.26	0.43	0.44	0.00	0.02	0.46	1.02	0.16	0.40	0.00	0.13	0.18	0.34	0.72	0.02
MgO	12.0	19.7	0.00	0.86	1.13	0.20	11.4	18.4	18.8	0.00	0.58	2.33	0.22	12.3	20.1	0.00	1.72	3.57	11.8	19.0	0.00
CaO	21.0	0.80	9.74	0.54	0.00	0.02	20.3	0.91	0.92	8.45	0.12	0.00	0.86	21.3	0.74	11.9	0.00	0.00	20.7	0.82	8.62
Na_2O	0.67	0.02	5.67	0.37	0.01	0.02	0.76	0.03	0.01	6.12	2.21	0.00	0.00	0.60	0.02	4.65	0.00	0.04	0.74	0.03	6.42
K_2O	0.00	0.00	0.82	15.1	0.02	0.00	0.00	0.01	0.00	1.11	13.5	0.00	0.01	0.01	0.01	0.39	0.00	0.00	0.00	0.00	0.59
NiO	0.01	0.02	0.01	0.01	0.00	0.00	0.01	0.00	0.00	0.02	0.02	0.00	0.03	0.00	0.03	0.01	0.05	0.00	0.03	0.01	0.01
Total	99.5	99.3	99.6	100.1	98.1	95.4	99.4	99.4	100.1	100.1	99.8	99.3	91.4	99.4	99.2	99.5	94.0	97.4	100.0	100.7	99.3
[O]=	6	6	8	8	3	3	6	6	6	8	8	3	3	6	6	8	3	3	6	6	8
Si	1.923	1.938	2.544	2.752	0.000	0.004	1.921	1.945	1.944	2.618	2.915	0.001	0.052	1.921	1.937	2.443	0.003	0.001	1.930	1.936	2.591
Al	0.144	0.093	1.437	1.254	0.001	0.045	0.156	0.098	0.093	1.361	1.073	0.002	0.079	0.153	0.105	1.536	0.101	0.005	0.127	0.077	1.395
Ti	0.008	0.002	0.000	0.018	0.972	0.489	0.009	0.003	0.002	0.000	0.000	0.946	0.380	0.009	0.002	0.001	0.215	0.884	0.007	0.003	0.000
Cr	0.001	0.000	0.000	0.000	0.001	0.006	0.001	0.000	0.000	0.000	0.000	0.000	0.007	0.000	0.001	0.000	0.006	0.001	0.001	0.001	0.001
Fe	0.358	0.810	0.008	0.029	1.007	1.917	0.395	0.854	0.851	0.016	0.018	1.004	1.937	0.327	0.778	0.011	2.311	1.075	0.391	0.872	0.007
Fe^{3+}	0.063	0.041					0.057	0.014						0.046	0.026				0.079	0.070	
Fe^{2+}	0.293	0.767					0.337	0.839						0.280	0.750				0.309	0.796	
Mn	0.007	0.016	0.001	0.000	0.002	0.010	0.008	0.014	0.014	0.000	0.001	0.010	0.029	0.005	0.013	0.000	0.004	0.004	0.011	0.023	0.001
Mg	0.677	1.119	0.000	0.060	0.044	0.010	0.644	1.051	1.066	0.000	0.040	0.088	0.011	0.692	1.140	0.000	0.087	0.140	0.664	1.076	0.000
Ca	0.853	0.033	0.473	0.027	0.000	0.001	0.828	0.037	0.038	0.407	0.006	0.000	0.030	0.863	0.030	0.580	0.000	0.000	0.841	0.033	0.418
Na	0.049	0.001	0.498	0.033	0.001	0.001	0.056	0.002	0.001	0.534	0.195	0.000	0.000	0.044	0.001	0.411	0.000	0.002	0.055	0.002	0.563
K	0.000	0.000	0.047	0.893	0.001	0.000	0.000	0.001	0.000	0.063	0.795	0.000	0.000	0.001	0.001	0.022	0.000	0.000	0.000	0.000	0.034
Ni	0.000	0.001	0.000	0.000	0.000	0.000	0.000	0.000	0.000	0.001	0.000	0.000	0.001	0.000	0.001	0.000	0.001	0.000	0.001	0.000	0.000
Sum	4.02	4.01	5.01	5.07	2.03	2.48	4.02	4.00	4.01	5.00	5.04	2.05	2.53	4.02	4.01	5.00	2.73	2.11	4.03	4.02	5.01
$Mg^{\#}$	0.65	0.58					0.62	0.55	0.56					0.68	0.59				0.63	0.55	
$Cr^{\#}$	0.00						0.01							0.00					0.01		
An			0.49							0.43						0.59					0.43
Or				0.94							0.80										

Table 2 (*Continued*)

	Type I			Type II																		
Sample	TY1b			TY7d								T15				TY65					TY16		
Rock	Quartz ganulite			Quartz ganulite								Garnet ganulite				Garnet granulite					Pyroxenes granulite		
Mineral	Qtz	Ilm	Hem	Cpx	Opx	Pl	Qtz	Kfs	Bt	Ilm	Hem	Cpx	Opx	Pl	Grt	Cpx	Opx	Pl	Grt	Pl	Cpx	$Cpx_{(I)}$	Opx
Points	5	5	5	5	5	5	5	3	5	5	5	5	5	5	5	5	5	5	5	inGrt	5	3	5
SiO_2	99.8	0.01	0.11	50.9	51.1	56.0	99.1	63.3	36.5	0.02	0.16	49.8	50.8	57.0	40.0	49.9	50.8	53.6	40.1	48.9	50.2	50.7	51.0
TiO_2	0.00	51.1	22.7	0.29	0.10	0.01	0.02	0.01	5.92	52.1	24.1	0.87	0.11	0.04	0.13	0.78	0.09	0.07	0.12	0.09	0.53	0.28	0.17
Al_2O_3	0.05	0.02	1.92	3.28	2.15	26.6	0.02	19.4	14.2	0.06	2.74	6.07	2.42	26.6	21.9	5.85	2.19	28.1	21.8	30.4	4.24	3.96	2.88
Cr_2O_3	0.02	0.00	0.03	0.03	0.02	0.03	0.03	0.04	0.04	0.02	0.31	0.07	0.02	0.02	0.04	0.01	0.02	0.06	0.05	0.04	0.04	0.00	0.02
FeO	0.02	46.3	67.9	11.1	25.1	0.22	0.17	1.03	17.8	42.8	61.8	9.97	24.6	0.17	19.4	10.1	25.4	0.59	19.1	2.45	11.1	12.0	23.0
MnO	0.03	0.91	0.77	0.26	0.44	0.00	0.01	0.00	0.12	0.57	0.34	0.13	0.47	0.03	0.52	0.13	0.49	0.00	0.58	0.06	0.26	0.35	0.39
MgO	0.00	1.03	0.28	12.0	19.9	0.00	0.00	1.01	11.3	2.64	1.05	11.7	20.1	0.00	13.1	12.13	19.8	0.00	13.1	0.36	12.0	11.9	20.8
CaO	0.00	0.09	0.08	20.9	0.80	9.57	0.03	0.41	0.01	0.02	0.09	19.9	0.87	9.21	4.93	19.3	0.81	11.6	4.79	12.3	19.7	20.9	0.98
Na_2O	0.00	0.01	0.02	0.68	0.03	5.72	0.01	0.50	0.78	0.00	0.02	1.04	0.04	6.09	0.04	1.04	0.03	4.84	0.08	3.99	0.87	0.77	0.07
K_2O	0.02	0.01	0.00	0.01	0.02	0.77	0.01	14.2	8.86	0.01	0.02	0.00	0.01	0.51	0.00	0.00	0.01	0.40	0.00	0.16	0.01	0.01	0.01
NiO	0.07	0.00	0.01	0.02	0.02	0.01	0.00	0.02	0.01	0.00	0.02	0.04	0.02	0.01	0.00	0.00	0.02	0.00	0.00	0.00	0.02	0.03	0.01
Total	100.0	99.5	93.8	99.4	99.6	98.9	99.4	100.0	95.5	98.3	90.6	99.7	99.4	99.7	100.0	99.2	99.7	99.2	99.7	98.8	99.1	100.9	99.3
[O]=	2	3	3	6	6	8	2	8	22	3	3	6	6	8	12	6	6	8	12	8	6	6	6
Si	0.999	0.000	0.004	1.926	1.940	2.552	0.998	2.920	5.526	0.001	0.005	1.866	1.929	2.572	2.991	1.875	1.933	2.452	3.006	2.280	1.905	1.922	1.924
Al	0.001	0.001	0.070	0.146	0.096	1.428	0.000	1.056	2.530	0.002	0.101	0.268	0.108	1.413	1.932	0.259	0.098	1.515	1.922	1.673	0.190	0.132	0.128
Ti	0.000	0.977	0.533	0.008	0.003	0.000	0.000	0.000	0.675	0.990	0.569	0.025	0.003	0.001	0.007	0.022	0.003	0.002	0.007	0.003	0.015	0.008	0.005
Cr	0.000	0.000	0.001	0.001	0.001	0.001	0.000	0.001	0.005	0.000	0.008	0.002	0.000	0.001	0.002	0.000	0.000	0.002	0.003	0.001	0.001	0.000	0.001
Fe	0.000	0.984	1.785	0.351	0.795	0.009	0.001	0.040	2.258	0.904	1.626	0.313	0.782	0.007	1.218	0.317	0.809	0.023	1.203	0.095	0.352	0.380	0.726
Fe^{3+}				0.051	0.031							0.036	0.046		0.112	0.034	0.050		0.090		0.049		0.027
Fe^{2+}				0.299	0.762							0.276	0.732		1.097	0.282	0.755		1.105		0.302		0.697
Mn	0.000	0.020	0.020	0.008	0.014	0.000	0.000	0.000	0.015	0.012	0.009	0.004	0.015	0.001	0.033	0.004	0.016	0.000	0.037	0.002	0.008	0.011	0.013
Mg	0.000	0.039	0.014	0.679	1.125	0.000	0.000	0.070	2.549	0.099	0.049	0.656	1.139	0.000	1.455	0.679	1.122	0.000	1.456	0.025	0.678	0.671	1.167
Ca	0.000	0.003	0.003	0.846	0.032	0.467	0.000	0.020	0.001	0.000	0.003	0.801	0.035	0.445	0.395	0.779	0.033	0.567	0.385	0.615	0.802	0.851	0.040
Na	0.000	0.000	0.001	0.050	0.002	0.505	0.000	0.044	0.229	0.000	0.001	0.076	0.003	0.532	0.005	0.076	0.002	0.429	0.012	0.361	0.064	0.056	0.005
K	0.000	0.000	0.000	0.000	0.001	0.045	0.000	0.836	1.713	0.000	0.001	0.000	0.000	0.029	0.000	0.000	0.000	0.023	0.000	0.009	0.000	0.000	0.001
Ni	0.001	0.000	0.000	0.001	0.001	0.000	0.000	0.002	0.001	0.000	0.001	0.001	0.001	0.000	0.000	0.000	0.001	0.000	0.000	0.000	0.001	0.001	0.000
Sum	1.00	2.02	2.43	4.02	4.01	5.01	1.00	4.99	15.50	2.01	2.37	4.01	4.02	5.00	8.04	4.01	4.02	5.01	8.03	5.07	4.02	4.03	4.01
$Mg^{\#}$				0.66	0.59				0.53			0.68	0.59		0.54	0.68	0.58		0.55		0.66	0.64	0.62
$Cr^{\#}$				0.01								0.01									0.01		
An						0.48								0.46				0.56		0.62			
Or								0.93															
Mg/Fe									1.13														

Type II

Sample	TY16		TY17				TY61									TY12							
Rock	Pyroxenes granulite		Pyroxenes granulite				Pyroxenes granulite									Olivine granulite							
Mineral	Pl	Ilm	Cpx	Opx	Pl	Ilm	Cpx	Opx	Pl	Ap	Kfs	Ilm	Hem	Ilm	Hem	Cpx	Opx	$Opx_{(I)}$	Pl	Ol	Kfs	Ilm	Hem
Points	5	5	5	5	5	5	5	5	5	5	3	5	5	in Pl	in Pl	5	5	3	5	5	3	5	5
SiO_2	57.9	0.02	50.4	50.8	58.8	0.02	50.8	50.5	55.1	0.08	64.4	0.01	0.07	0.00	0.07	50.2	50.5	50.7	58.1	35.2	63.7	0.00	0.04
TiO_2	0.03	52.1	0.96	0.09	0.05	50.3	0.34	0.09	0.01	0.01	0.01	53.3	27.7	52.0	20.7	0.36	0.09	0.08	0.01	0.00	0.01	49.3	19.5
Al_2O_3	25.8	0.20	3.71	2.14	25.7	0.15	3.56	2.57	27.6	0.00	19.2	0.05	2.21	0.01	1.83	4.22	2.55	2.52	26.1	0.00	19.1	0.10	3.09
Cr_2O_3	0.02	0.14	0.01	0.02	0.02	0.11	0.02	0.00	0.01	0.04	0.03	0.03	0.16	0.04	0.22	0.01	0.01	0.00	0.00	0.00	0.02	0.04	0.03
FeO	0.24	42.6	9.99	25.4	0.20	44.1	11.1	24.7	0.21	0.35	0.61	41.8	62.5	45.6	71.0	11.2	23.6	23.8	0.24	35.6	0.52	45.0	72.0
MnO	0.02	0.73	0.18	0.55	0.01	0.52	0.25	0.46	0.01	0.03	0.02	0.30	1.07	0.22	0.29	0.46	0.48	0.39	0.01	0.83	0.00	0.69	0.74
MgO	0.00	3.11	13.1	20.2	0.00	3.03	11.9	19.8	0.00	0.00	0.51	4.03	0.00	1.77	0.63	11.8	21.7	21.5	0.00	28.8	0.51	3.41	2.09
CaO	8.40	0.01	20.7	0.80	8.00	0.03	21.1	0.90	10.5	55.3	0.29	0.00	0.00	0.02	0.05	20.5	0.78	0.75	8.23	0.31	0.23	0.02	0.00
Na_2O	6.43	0.03	0.53	0.03	6.93	0.01	0.64	0.04	5.32	0.08	2.33	0.00	0.00	0.00	0.01	1.03	0.04	0.03	6.75	0.00	0.56	0.01	0.03
K_2O	0.75	0.00	0.01	0.01	0.48	0.00	0.01	0.01	0.69	0.01	12.3	0.00	0.00	0.01	0.02	0.00	0.00	0.00	0.57	0.00	14.6	0.00	0.01
NiO	0.03	0.02	0.01	0.02	0.01	0.00	0.04	0.06	0.03	0.01	0.03	0.08	0.01	0.00	0.08	0.01	0.03	0.00	0.03	0.00	0.03	0.04	0.02
Total	99.6	99.0	99.6	100.0	100.2	98.3	99.7	99.1	99.5	55.9	99.8	99.6	93.7	99.7	94.9	99.8	99.7	99.7	100.0	100.7	99.3	98.6	97.5
[O]=	8	3	6	6	8	3	6	6	8	1	8	3	3	3	3	6	6	6	8	4	8	3	3
Si	2.610	0.001	1.895	1.927	2.628	0.001	1.918	1.926	2.502	0.001	2.951	0.000	0.002	0.000	0.002	1.897	1.906	1.912	2.608	0.978	2.953	0.000	0.002
Al	1.372	0.006	0.164	0.096	1.356	0.004	0.159	0.115	1.480	0.000	1.038	0.001	0.079	0.000	0.068	0.188	0.114	0.112	1.378	0.000	1.045	0.003	0.111
Ti	0.001	0.981	0.027	0.003	0.002	0.962	0.010	0.003	0.000	0.000	0.000	0.989	0.631	0.984	0.489	0.010	0.003	0.002	0.000	0.000	0.000	0.945	0.445
Cr	0.001	0.003	0.000	0.001	0.001	0.002	0.001	0.000	0.000	0.001	0.001	0.001	0.004	0.001	0.006	0.000	0.000	0.000	0.000	0.000	0.001	0.001	0.001
Fe	0.009	0.891	0.314	0.804	0.008	0.938	0.351	0.787	0.008	0.005	0.024	0.863	1.582	0.959	1.866	0.353	0.745	0.750	0.009	0.825	0.020	0.959	1.826
Fe^{3+}			0.044	0.070			0.049	0.046								0.108	0.109						
Fe^{2+}			0.269	0.729			0.300	0.737								0.242	0.629						
Mn	0.001	0.016	0.006	0.017	0.000	0.011	0.008	0.015	0.001	0.000	0.001	0.006	0.028	0.005	0.008	0.015	0.015	0.013	0.000	0.019	0.000	0.015	0.019
Mg	0.000	0.116	0.735	1.140	0.000	0.115	0.670	1.128	0.000	0.000	0.035	0.148	0.000	0.066	0.029	0.667	1.219	1.210	0.000	1.191	0.035	0.130	0.095
Ca	0.406	0.000	0.835	0.032	0.383	0.001	0.853	0.037	0.510	0.990	0.014	0.000	0.000	0.001	0.002	0.830	0.031	0.030	0.396	0.009	0.011	0.000	0.000
Na	0.562	0.002	0.038	0.002	0.601	0.000	0.047	0.003	0.468	0.003	0.206	0.000	0.000	0.000	0.001	0.076	0.003	0.002	0.588	0.000	0.050	0.000	0.002
K	0.043	0.000	0.000	0.000	0.027	0.000	0.001	0.001	0.040	0.000	0.721	0.000	0.000	0.000	0.001	0.000	0.000	0.000	0.033	0.000	0.867	0.000	0.000
Ni	0.001	0.000	0.000	0.001	0.001	0.000	0.001	0.002	0.001	0.000	0.001	0.002	0.000	0.000	0.002	0.000	0.001	0.000	0.001	0.000	0.001	0.001	0.001
Sum	5.01	2.02	4.01	4.02	5.01	2.03	4.02	4.02	5.01	1.00	4.99	2.01	2.33	2.02	2.47	4.04	4.04	4.03	5.01	3.02	4.98	2.05	2.50
$Mg^{\#}$			0.70	0.59			0.66	0.59								0.65	0.62	0.62		0.59			
$Cr^{\#}$			0.00				0.00									0.00							
An	0.42				0.39				0.52										0.40				
Or											0.77										0.93		

Hem is the lamellae in Ilm; $Opx_{(I)}$ and $Cpx_{(I)}$: relict mineral in petrography.

Table 3
Representative major elements (wt%) and Lu–Hf isotopes analyses of zircons from the Tuoyun granulite xenoliths

Type	Sample	HfO_2 (wt%)	Y_2O_3 (wt%)	Y/Hf	Ex-shape	Cr-shape	C-zoning	$^{176}Hf/^{177}Hf$	1 S.D.	$^{176}Lu/^{176}Hf$	$^{176}Yb/^{176}Hf$	Age (Ma)	Hf_i[a)]	Epsilon	1s	$T_{(DM)}$ (Ga)	$T_{(crust)}$ (Ga)
Type 1	TY62																
	TY62-1	1.67	0.01	0.01	S	I	I	0.282203	0.000021	0.000602	0.025966	853	0.282193	−1.6	0.7	1.5	1.9
	TY62-3	1.25	0.23	0.17	S	S	N	0.282219	0.000021	0.000944	0.042092	836	0.282204	−1.6	0.7	1.5	1.8
	TY62-4	1.35	0.14	0.10	I		N	0.282104	0.000015	0.000946	0.043653	722	0.282091	−8.2	0.5	1.6	2.2
	TY62-5	1.15	0.18	0.15	R		N	0.282169	0.000012	0.001004	0.044737	672	0.282156	−7.0	0.4	1.5	2.1
	TY62-6	1.37	0.17	0.12	S	S	N	0.282190	0.000017	0.001396	0.064246	635	0.282173	−7.2	0.6	1.5	2.0
	TY62-7	1.27	0.02	0.01	R		N	0.281990	0.000016	0.000202	0.008779	584	0.281988	−14.9	0.6	1.7	2.5
	TY62-8	1.19	0.15	0.12	S		N	0.282134	0.000014	0.001330	0.061272	956	0.282110	−2.3	0.5	1.6	2.0
	TY62-9	1.39	0.07	0.05	S	E	N	0.282189	0.000013	0.000797	0.035825	525	0.282181	−9.4	0.5	1.5	2.1
	TY62-10	1.60	0.01	0.01	S	R	I	0.282144	0.000015	0.000690	0.029532	662	0.282135	−7.9	0.5	1.5	2.1
	TY62-11C	1.08	0.01	0.01	R	S	N	0.282097	0.000018	0.000995	0.043484	885	0.282080	−4.9	0.6	1.6	2.1
	TY62-12	1.05	0.10	0.09	R	S	N	0.282126	0.000013	0.000768	0.034570	723	0.282116	−7.3	0.5	1.6	2.1
	TY62-13	1.21	0.15	0.12	R	S	L	0.282204	0.000015	0.000588	0.025922	809	0.282195	−2.6	0.5	1.5	1.9
	TY62-15	1.26	0.17	0.13	S	E	L	0.282157	0.000013	0.000796	0.035577	749	0.282146	−5.6	0.5	1.5	2.0
	TY62-16	1.77	0.03	0.02	S		N	0.282158	0.000013	0.000736	0.033409	758	0.282148	−5.4	0.5	1.5	2.0
	TY62-17	1.41	0.10	0.07	I	S	L	0.282107	0.000013	0.000857	0.038647	809	0.282094	−6.1	0.5	1.6	2.1
	TY62-18R	1.29	0.08	0.06				0.282164	0.000013	0.000843	0.035225	858	0.282150	−3.0	0.5	1.5	1.9
	TY67																
	TY67-048	1.28	0.27	0.20	I		N	0.282209	0.000013	0.001011	0.045908	662	0.282196	−5.8	0.5	1.5	2.0
	TY67-049	1.10	0.20	0.17	R		N	0.282261	0.000011	0.001327	0.062425	606	0.282246	−5.3	0.4	1.4	1.9
	TY67-050	1.11	0.00	0.00	I		N	0.282203	0.000013	0.001908	0.093979	246	0.282194	−15.0	0.5	1.5	2.2
	TY67-052	1.24	0.28	0.21	I		N	0.282216	0.000012	0.001835	0.087541	678	0.282193	−5.6	0.4	1.5	2.0
	TY67-053	1.47	0.07	0.04	I		N	0.282275	0.000013	0.000672	0.030489	768	0.282265	−1.0	0.5	1.4	1.7
	TY67-056	1.35	0.11	0.08	I		N	0.282248	0.000013	0.001098	0.051378	547	0.282237	−6.9	0.5	1.4	2.0
	TY67-057	1.18	0.13	0.10	I		N	0.282268	0.000012	0.000813	0.039880	299	0.282263	−11.4	0.4	1.4	2.0
	TY67-060	1.39	0.39	0.26	I		N	0.282181	0.000011	0.000613	0.032574	698	0.282173	−5.8	0.4	1.5	2.0
	TY67-063	1.36	0.06	0.04	I		N	0.282287	0.000012	0.000739	0.037120	629	0.282278	−3.6	0.4	1.4	1.8
	TY67-064	1.40	0.04	0.02	I		N	0.282231	0.000011	0.000705	0.034572	619	0.282223	−5.8	0.4	1.4	1.9
	TY67-065	1.11	0.13	0.11	I		N	0.282239	0.000012	0.000596	0.029950	551	0.282233	−6.9	0.4	1.4	2.0
	TY67-067	1.32	0.10	0.07	I		N	0.282281	0.000013	0.001036	0.049101	530	0.282271	−6.1	0.5	1.4	1.9
	TY67-069	1.28	0.09	0.07	I		N	0.282214	0.000013	0.000716	0.035915	523	0.282207	−8.5	0.5	1.5	2.0
	TY67-070	1.31	0.14	0.10	I		N	0.282190	0.000009	0.000705	0.034673	597	0.282182	−7.7	0.3	1.5	2.0
	TY67-071	1.42	0.12	0.08	I	I	N	0.282251	0.000016	0.001476	0.075644	505	0.282237	−7.8	0.6	1.4	2.0
	TY67-077	1.30	0.13	0.09	I		N	0.282242	0.000012	0.000945	0.046053	556	0.282232	−6.9	0.4	1.4	2.0
	TY67-079	1.38	0.21	0.14	I		N	0.282257	0.000012	0.001387	0.069871	521	0.282243	−7.2	0.4	1.4	2.0
	TY67-082	1.03	0.26	0.23	I		N	0.282281	0.000012	0.001369	0.070050	587	0.282266	−5.0	0.4	1.4	1.9
	TY67-083	1.31	0.00	0.00	I		N	0.282242	0.000011	0.000700	0.034884	569	0.282235	−6.5	0.4	1.4	1.9
	TY16																
Type II	TY16-223	1.20	0.05	0.03	R		N	0.281977	0.000012	0.000158	0.007254	122	0.281977	−25.5	0.4	1.8	2.8
	TY16-225	1.14	0.02	0.01	S		N	0.281991	0.000011	0.000185	0.008258	230	0.281990	−22.6	0.4	1.7	2.7
	TY16-226	1.21	0.03	0.02	R		N	0.282013	0.000012	0.000204	0.009084	547	0.282011	−14.9	0.4	1.7	2.5

TY16-227	1.08	0.04	0.03	I		N	0.282008	0.000010	0.000291	0.012674	340	0.282006	−19.6	0.3	1.7	2.6
TY16-228	1.12	0.00	0.00	I		N	0.282045	0.000009	0.000318	0.014513	231	0.282044	−20.7	0.3	1.7	2.6
TY16-229	1.28	0.12	0.08	R		N	0.282083	0.000010	0.000497	0.021534	355	0.282080	−16.7	0.3	1.6	2.4
TY16-230	1.16	0.01	0.01	R		N	0.282060	0.000011	0.000165	0.007310	507	0.282058	−14.1	0.4	1.6	2.4
TY16-028	1.32	0.04	0.03	R		N	0.282172	0.000010	0.000651	0.028263	529	0.282166	−9.8	0.4	1.5	2.1
TY16-029	1.23	0.02	0.02	I		N	0.282057	0.000009	0.000516	0.022251	133	0.282056	−22.4	0.3	1.7	2.6
TY16-030R	1.02	0.06	0.05	I		N	0.282113	0.000016	0.000537	0.023041	299	0.282110	−16.9	0.6	1.6	2.4
TY16-030C							0.282061	0.000013	0.000276	0.011788	544	0.282058	−13.3	0.5	1.6	2.3
TY16-031	1.17	0.03	0.03	R	S	N	0.281996	0.000010	0.000160	0.006902	471	0.281995	−17.2	0.3	1.7	2.5
TY16-033	1.01	0.02	0.02	S		N	0.282027	0.000013	0.000283	0.012003	511	0.282024	−15.2	0.5	1.7	2.4
TY16-034	1.16	0.06	0.05	I		N	0.281982	0.000010	0.000176	0.007484	716	0.281980	−12.3	0.3	1.7	2.4
TY16-035	1.17	0.04	0.03	S		N	0.281979	0.000017	0.000524	0.022704	142	0.281978	−25.0	0.6	1.8	2.8
TY16-036R	1.15	0.06	0.05	R		N	0.282091	0.000019	0.000561	0.024369	119	0.282090	−21.5	0.7	1.6	2.5
TY16-036C							0.281838	0.000013	0.000713	0.030227	283	0.281834	−27.0	0.5	2.0	3.0
TY16-037	1.35	0.01	0.01	I		N	0.282001	0.000015	0.000177	0.007655	123	0.282001	−24.6	0.5	1.7	2.7
TY16-038	1.12	0.10	0.08	I		N	0.282034	0.000011	0.000416	0.017965	154	0.282033	−22.8	0.4	1.7	2.6
TY16-039	1.26	0.04	0.03	I		N	0.282058	0.000014	0.000288	0.012691	168	0.282057	−21.6	0.5	1.7	2.6
TY16-040	1.24	0.04	0.03	I		N	0.282036	0.000013	0.000270	0.011608	680	0.282033	−11.2	0.5	1.7	2.3
TY61																
TY61-001	1.10	0.00	0.00	I		N	0.282281	0.000008	0.000346	0.014605	115	0.282280	−14.9	0.3	1.3	2.1
TY61-002	0.77	0.08	0.10	I		N	0.282313	0.000009	0.000369	0.016687	374	0.282310	−8.1	0.3	1.3	1.9
TY61-003	1.04	0.03	0.03	I		N	0.282249	0.000009	0.000348	0.014760	209	0.282248	−14.0	0.3	1.4	2.1
TY61-004	0.88	0.00	0.00	I		N	0.282255	0.000010	0.000374	0.015701	550	0.282251	−6.3	0.3	1.4	1.9
TY61-005	0.97	0.05	0.05	I		N	0.282268	0.000009	0.000413	0.017095	673	0.282263	−3.2	0.3	1.4	1.8
TY61-006	1.61	0.02	0.01	I		N	0.282258	0.000008	0.000478	0.020403	687	0.282252	−3.3	0.3	1.4	1.8
TY61-009	1.43	0.01	0.01	I		N	0.282283	0.000010	0.000438	0.017574	456	0.282279	−7.4	0.3	1.3	1.9
TY61-010	1.42	0.04	0.03	I		N	0.282258	0.000010	0.000507	0.020241	561	0.282253	−6.0	0.3	1.4	1.9
TY61-011	1.28	0.12	0.09	S		O	0.282632	0.000008	0.000551	0.024790	161	0.282630	−1.5	0.3	0.9	1.3
TY61-013	1.02	0.02	0.02	R		N	0.282243	0.000009	0.000435	0.018474	695	0.282237	−3.6	0.3	1.4	1.9
TY61-014	1.03	0.01	0.01	I		N	0.282278	0.000011	0.000387	0.015482	53	0.282278	−16.3	0.4	1.4	2.2
TY61-015	1.11	0.00	0.00	I		N	0.282276	0.000011	0.000347	0.014113	51	0.282276	−16.4	0.4	1.4	2.2
TY61-016	0.98	0.01	0.01	I		N	0.282272	0.000009	0.000316	0.013259	615	0.282268	−4.3	0.3	1.4	1.8
TY61-017	1.13	0.07	0.06	I		N	0.282330	0.000010	0.000430	0.017616	155	0.282329	−12.3	0.3	1.3	2.0
TY61-018	1.09	0.00	0.00	I		N	0.282241	0.000011	0.000437	0.018369	116	0.282240	−16.3	0.4	1.4	2.2
TY61-019	0.99	0.07	0.06	I		N	0.282259	0.000011	0.000366	0.015487	572	0.282255	−5.7	0.4	1.4	1.9
TY61-020	0.91	0.04	0.04	I		N	0.282270	0.000013	0.000227	0.009932	435	0.282268	−8.3	0.5	1.4	1.9
TY61-021	0.88	0.08	0.08	I		N	0.282279	0.000010	0.000376	0.016352	595	0.282275	−4.5	0.3	1.4	1.8
TY61-022	0.84	0.04	0.04	I		N	0.282312	0.000011	0.000332	0.014290	566	0.282308	−3.9	0.4	1.3	1.8
TY61-023	1.60	0.10	0.06	I		N	0.282284	0.000009	0.001045	0.049256	160	0.282281	−13.9	0.3	1.4	2.1
TY61-027	1.08	0.00	0.00	I		N	0.282273	0.000016	0.000323	0.014620	615	0.282269	−4.2	0.6	1.4	1.8

Hfi, Initial Hf-isotope composition for U–Pb age; ^{176}Lu decay constant is 1.865×10^{-11}. Shape: R, rounded; I, irregular; S, subhedral; E, euhedral; Zoning: O-Oscillatory, L, lamellar; I, irregular; N-No internal structure; Ex-external; Cr-core.

Table 4
Major element compositions of Tuoyun granulite xenoliths (wt%)

	Type I						Type II			
Sample	TY13	TY62	TY67	TY1b	TY7d	TY15	TY12	TY16	TY17	TY61
Rock type	PG	PG	PG	QG	QG	GG	OG	PG	PG	PG
SiO_2	53.3	51.1	48.7	56.8	52.2	48.2	50.3	52.0	47.1	46.1
TiO_2	0.97	1.15	0.86	0.88	0.85	0.85	1.40	1.12	1.41	1.67
Al_2O_3	17.4	17.4	16.5	17.6	17.0	18.3	19.6	18.6	17.2	18.9
Fe_2O_3	2.19	3.18	2.89	2.13	2.17	2.73	2.55	2.07	3.65	3.18
FeO	6.51	7.45	8.61	5.70	6.66	7.69	6.00	5.94	8.40	7.96
MnO	0.14	0.15	0.14	0.12	0.14	0.14	0.13	0.11	0.16	0.20
MgO	5.30	5.56	8.26	3.70	5.86	6.84	5.05	5.49	8.03	6.64
CaO	8.44	9.05	10.8	7.48	9.14	11.0	8.16	8.75	10.4	9.39
Na_2O	3.37	3.45	2.32	3.86	3.39	2.83	4.64	4.02	2.54	3.66
K_2O	1.68	0.81	0.22	0.99	1.24	0.49	1.41	0.52	0.59	1.70
P_2O_5	0.29	0.31	0.03	0.26	0.21	0.06	0.17	0.38	0.15	0.41
H_2O^+	0.17	0.12	0.17	0.13	0.19	0.17	0.21	0.16	0.20	0.14
CO_2	0.18	0.10	0.25	0.18	0.30	0.50	0.43	0.27	0.35	0.19
Total	100.0	99.9	99.8	99.8	99.4	99.7	100.1	99.5	100.2	100.1
$Mg^{\#}$	0.56	0.53	0.60	0.50	0.58	0.58	0.56	0.59	0.59	0.56
Q	1.08			8.26						
Or	9.92	4.79	1.30	5.85	7.33	2.89	8.33	3.07	3.49	10.04
Ab	28.5	29.2	19.6	32.7	28.7	23.9	34.2	34.0	21.5	18.1
Ne							2.76			6.97
An	27.4	29.6	34.0	27.8	27.5	35.8	28.5	31.2	33.8	30.1
Di	9.35	10.3	14.5	5.34	11.9	12.4	6.62	6.53	11.8	10.2
Hy	17.4	17.7	18.3	14.1	17.2	7.19		17.4	8.77	
Ol		0.39	5.43		0.64	10.6	11.8	0.47	11.5	15.4
Mt	3.18	4.61	4.19	3.09	3.15	3.96	3.70	3.00	5.29	4.61
Il	1.84	2.18	1.63	1.67	1.61	1.61	2.66	2.13	2.68	3.17
Ap	0.69	0.73	0.07	0.62	0.50	0.14	0.40	0.90	0.36	0.97
Cc	0.41	0.23	0.57	0.41	0.68	1.14	0.98	0.61	0.80	0.43
A (wt%)	26.5	20.8	11.4	29.6	24.0	16.1	30.8	25.2	13.5	23.2
F	45.7	52.0	51.6	47.8	45.7	50.6	43.5	44.4	51.9	48.1
M	27.8	27.2	37.0	22.6	30.3	33.2	25.7	30.4	34.6	28.7
Series	CA	CA	LK-TH	CA	CA	CA	ALK	LK-TH	CA	ALK

PG, Pyroxenes granulite; OG, olivine granulite; Q, quartz granulite; GG, garnet granulite; ALK, alkalic; CA, calc-alkalic; LK-TH, low potassium tholeittic.

were calculated for each mass sweep and the time-resolved ratios for each analysis were then carefully examined. Optimal signal intervals for the background and ablation data were selected for each sample and automatically matched with identical time intervals for the standard zircon analyses, thus correcting for the effects of ablation/transport-related U/Pb fractionation and mass bias of the mass spectrometer. Net background-corrected count rates for each isotope were used for calculation of sample ages. U and Th contents were estimated by direct comparison of integrated count rates with those on the GJ-1 standard.

The ^{204}Pb isotope cannot be precisely measured with this technique, due to a combination of low signal and interference from small amounts of Hg in the Ar gas supply. Common-Pb contents were therefore evaluated using the method described by Andersen (2002); these were negligible in nearly all samples. Concordia ages were determined using Isoplot 2.32 (Ludwig, 2000).

3.4. Hf-isotope analysis of zircon

Hf-isotope analyses were carried out in situ with a Merchantek EO LUV 213 nm laser-ablation microprobe, attached to a Nu Plasma multi-collector (MC-) ICPMS at GEMOC, using techniques described in detail by Griffin et al. (2000, 2002). Interference of ^{176}Lu on ^{176}Hf has been corrected by measuring the intensity of the interference-free ^{175}Lu isotope, using the recommended $^{176}Lu/^{175}Lu = 0.02669$ (Debievre and Taylor, 1993) to calculate $^{176}Lu/^{177}Hf$. Similarly, the interference of ^{176}Yb on ^{176}Hf has been corrected by

Table 5
Trace element concentrations of the Tuoyun granulite xenoliths (ppm)

	Type I						Type II				P.M.
Sample	TY13	TY62	TY67	TY1b	TY7d	TY15	TY12	TY16	TY17	TY61	
Rock type	PG	PG	PG	QG	QG	GG	OG	PG	PG	PG	
La	18.3	21.1	5.07	16.5	15.9	4.33	13.9	20.6	7.47	31.2	0.648
Ce	39.6	47.3	10.8	35.2	33.0	10.9	29.3	43.4	18.7	63.0	1.675
Pr	4.80	6.40	1.48	4.66	4.20	1.79	4.22	5.24	2.69	7.82	0.254
Nd	19.4	27.6	6.68	20.0	16.9	8.68	19.3	21.5	12.2	32.4	1.25
Sm	3.80	6.49	1.80	4.44	3.69	2.53	4.86	4.52	3.41	6.89	0.406
Eu	1.22	1.66	0.75	1.49	1.23	0.98	1.80	1.77	1.26	2.44	0.154
Tb	0.52	0.95	0.30	0.67	0.54	0.46	0.74	0.68	0.62	0.97	0.099
Gd	3.56	6.34	1.90	4.39	3.54	2.87	4.84	4.61	3.79	6.49	0.544
Dy	2.89	5.43	1.85	3.97	3.03	2.91	4.19	3.86	3.73	5.28	0.674
Ho	0.59	1.09	0.37	0.81	0.63	0.61	0.84	0.76	0.77	1.07	0.149
Er	1.62	2.98	1.08	2.13	1.75	1.74	2.18	2.05	2.14	2.93	0.438
Yb	1.46	2.47	0.93	1.87	1.58	1.56	1.75	1.78	1.90	2.43	0.441
Lu	0.21	0.36	0.14	0.26	0.22	0.23	0.23	0.27	0.27	0.35	0.0675
Sc	25.4	32.2	36.8	20.7	28.8	36.9	26.9	20.6	27.1	25.3	16.2
V	242	238	339	170	220	277	231	171	242	224	82.0
Cr	61.9	76.6	95.1	19.8	92.4	170	88.8	91.8	85.1	60.3	2625
Co	27.4	27.4	38.7	19.7	29.8	37.6	29.0	31.9	49.6	36.3	105
Ni	32.4	21.1	54.9	10.4	41.2	45.9	64.2	135	160	45.3	1960
Cu	55.2	33.8	135	15.5	18.4	43.1	44.2	200	61.3	25.8	30
Zn	74.8	97.8	75.9	77.7	76.3	68.5	68.9	64.0	82.4	115	55
Ga	19.1	21.6	18.5	19.6	19.4	18.2	21.6	20.0	18.1	20.9	194
Rb	23.3	3.97	1.73	6.33	21.2	5.69	12.1	2.46	5.73	23.4	0.6
Sr	627	587	589	652	656	544	879	623	420	908	19.9
Y	17.3	30.1	10.4	21.4	17.3	17.7	22.2	22.7	22.3	29.1	4.3
Zr	21.4	56.6	17.4	27.1	34.2	35.7	104	101	88.8	153	10.5
Nb	9.13	12.2	0.95	10.5	9.7	0.58	19.1	7.67	6.12	52.4	0.7
Ba	463	450	145	336	380	147	401	404	92.9	372	6.6
Hf	0.73	1.63	0.64	0.68	0.94	1.18	2.58	2.49	2.19	3.17	0.283
Ta	0.51	0.55	0.05	0.43	0.46	0.04	0.93	0.32	0.37	2.85	0.037
Pb	7.32	5.71	2.12	4.32	6.03	1.87	3.30	5.19	2.25	7.13	0.15
Th	0.49	0.06	0.11	0.13	0.31	0.11	0.75	0.23	0.61	3.01	0.0795
U	0.17	0.08	0.12	0.08	0.10	0.12	0.26	0.24	0.28	0.84	0.0203
REE	98.0	130	33.1	96.5	86.1	39.6	88.1	111	59.0	163	6.80
Eu/Eu*	1.01	0.79	1.24	1.03	1.06	1.12	1.13	1.19	1.07	1.11	1.00
$(La/Yb)_n$	8.30	5.62	3.59	5.84	12.10	1.83	5.25	7.62	2.60	8.48	1.00
Th/U	2.96	0.81	0.99	1.66	3.21	0.90	2.85	0.96	2.17	3.59	3.92
Th/La	0.03	0.00	0.02	0.01	0.02	0.03	0.05	0.01	0.08	0.10	0.12
Ce/Pb	5.41	8.29	5.10	8.16	5.47	5.84	8.86	8.37	8.33	8.83	11.2
K/Rb	599	1674	1055	1299	486	714	959	1723	826	581	400
Ba/La	25.2	21.3	28.5	20.3	23.9	34.0	28.8	19.6	12.4	11.9	10.2
La/Nb	2.01	1.73	5.36	1.58	1.64	7.51	0.73	2.69	1.22	0.60	0.93
Nb/Y	0.53	0.40	0.09	0.49	0.56	0.03	0.86	0.34	0.27	1.80	0.16
Sr/Ba	1.35	1.31	4.08	1.94	1.73	3.69	2.19	1.54	4.52	2.44	3.02

P.M., Primitive mantle (McDonough and Sun, 1995); rock type is same as in Table 4.

measuring the interference-free ^{172}Yb isotope and using $^{176}Yb/^{172}Yb$ to calculate $^{176}Yb/^{177}Hf$. The appropriate value of $^{176}Yb/^{172}Yb$ was determined by spiking the JMC475 Hf standard with Yb, and determining the value of $^{176}Yb/^{172}Yb$ (0.58669) required to yield the value of $^{176}Hf/^{177}Hf$ obtained on the pure Hf solution. Most LAM analyses were carried out in He carrier gas with a beam diameter of ca. 30 μm, a 10 Hz repetition time and energies of 0.6–1.3 mJ/pulse. Typical ablation times were 80–120 s, resulting in pits 40–60 μm deep. For the calculation of ε_{Hf} values we have adopted the chondritic values of Blichert-Toft and Albarede (1998). The preci-

Table 6
U–Pb data for zircons from the Tuoyun granulite xenoliths

Type	Sample	Grain	Ex-shape	Cr-shape	C-zoning	Measured ratios								Th[a]	U[a]	Th/U	Corrected ages (Ma)								com-Pb
						$^{207}Pb/^{206}Pb$	1s	$^{207}Pb/^{235}U$	1s	$^{206}Pb/^{238}U$	1s	$^{208}Pb/^{232}Th$	1s				$^{207}Pb/^{206}Pb$	1s	$^{207}Pb/^{235}U$	1s	$^{206}Pb/^{238}U$	1s	$^{208}Pb/^{232}Th$	1s	%
	TY62	TY62-1	S	I	I	0.06274	0.00090	1.22226	0.01696	0.14141	0.00146	0.05078	0.00071	53	100	0.53	699	30	811	14	853	10	1001	14	0.0
		TY62-2	S		N	0.06612	0.00095	1.44215	0.02001	0.15836	0.00164	0.05771	0.00074	75	86	0.88	810	30	907	14	948	10	1134	13	0.0
		TY62-3	S	S	N	0.06706	0.00111	1.27813	0.02033	0.13839	0.00149	0.05296	0.00077	49	58	0.84	840	34	836	16	836	11	1043	15	0.0
		TY62-4	I		N	0.06685	0.00129	1.10086	0.02030	0.11957	0.00135	0.04210	0.00066	48	44	1.10	583	78	693	35	722	12	795	25	0.0
		TY62-5	R		N	0.06665	0.00137	1.01829	0.02008	0.11093	0.00128	0.03848	0.00077	25	40	0.63	538	78	647	34	672	12	687	32	0.0
		TY62-6	S	S	N	0.06962	0.00122	1.00835	0.01688	0.10513	0.00115	0.03904	0.00057	70	64	1.09	496	78	612	35	635	11	717	26	0.0
		TY62-7	R		N	0.06865	0.00246	0.90409	0.03101	0.09558	0.00144	0.03192	0.00117	8	14	0.56	691	119	610	56	584	15	580	60	0.0
		TY62-8	S		N	0.06378	0.00089	1.40463	0.01911	0.15979	0.00166	0.05331	0.00083	43	100	0.43	734	29	891	14	956	10	1050	16	0.0
		TY62-9	S	E	N	0.06127	0.00127	0.72155	0.01439	0.08543	0.00099	0.03048	0.00053	48	55	0.87	419	83	508	36	525	12	579	26	0.0
		TY62-10c	S	R	I	0.06210	0.00126	0.92585	0.01813	0.10813	0.00126	0.03616	0.00078	22	45	0.48	678	43	665	20	662	12	718	22	0.0
		TY62-10r				0.05955	0.00199	0.69570	0.02219	0.08450	0.00127	0.03272	0.00095	137	136	1.00	420	129	504	58	520	15	630	39	0.0
		TY62-11c	R	S	N	0.06224	0.00150	1.26628	0.02928	0.14707	0.00191	0.05628	0.00152	113	135	0.83	682	51	831	23	885	13	1107	27	0.0
		TY62-12	R	S	N	0.06132	0.00189	1.00889	0.02974	0.11889	0.00173	0.04756	0.00147	101	110	0.92	599	112	694	52	723	15	929	38	0.0
		TY62-13	R	S	L	0.06252	0.00225	1.15636	0.03962	0.13364	0.00216	0.05128	0.00190	72	84	0.85	692	75	780	34	809	16	1011	37	0.0
		TY62-14	S		N	0.06300	0.00332	0.44865	0.02242	0.05146	0.00106	0.02017	0.00098	72	82	0.88	227	217	312	98	319	21	359	76	0.0
		TY62-15	S	E	L	0.05971	0.00154	1.01761	0.02514	0.12317	0.00164	0.04515	0.00163	127	139	0.92	593	55	713	25	749	13	893	36	0.0
		TY62-16	S		N	0.08438	0.00322	1.50206	0.05368	0.12872	0.00236	0.05628	0.00258	38	47	0.81	566	170	727	80	758	19	874	85	0.0
		TY62-17	I	S	L	0.06683	0.00229	1.23429	0.04020	0.13364	0.00214	0.04777	0.00219	62	79	0.79	832	70	816	33	809	16	943	46	0.0
		TY62-18c	I	R	O	0.09843	0.00568	2.01269	0.10798	0.14808	0.00398	0.09748	0.00817	4	17	0.24	801	192	865	93	858	28	853	245	0.0
		TY62-18r				0.06245	0.00211	0.97064	0.03130	0.11265	0.00176	0.03645	0.00187	65	129	0.50	690	70	689	32	688	16	724	51	0.0
		TY62-19c	R	S	N	0.06339	0.00107	1.45371	0.02391	0.16638	0.00193	0.05237	0.00072	87	81	1.07	721	35	911	16	992	12	1032	14	0.0
		TY62-19r				0.06694	0.00127	1.51853	0.02794	0.16461	0.00198	0.05520	0.00111	24	50	0.48	836	39	938	18	982	12	1086	20	0.0
		TY62-20	I		N	0.06222	0.00091	0.97463	0.01376	0.11360	0.00122	0.03655	0.00042	106	97	1.09	682	31	691	14	694	11	726	11	0.0
		TY62-21	R	I	N	0.06723	0.00114	1.32608	0.02151	0.14306	0.00161	0.04688	0.00070	38	52	0.73	845	35	857	16	862	11	926	15	0.0
		TY62-22c	I	S	N	0.07646	0.00182	1.51666	0.03447	0.14388	0.00192	0.07534	0.00259	4	20	0.18	677	74	815	32	853	14	880	78	0.0
		TY62-22r				0.06247	0.00062	0.89792	0.00867	0.10425	0.00102	0.03143	0.00036	107	1224	0.09	690	21	651	10	639	10	625	11	0.0
		TY62-23	S		N	0.06335	0.00140	1.01531	0.02161	0.11628	0.00146	0.03627	0.00071	39	54	0.72	720	46	712	21	709	13	720	20	0.0
		TY62-24	R		N	0.06457	0.00075	1.17214	0.01352	0.13167	0.00138	0.04210	0.00044	218	320	0.68	656	45	761	18	795	11	803	16	0.0
		TY62-25	S	R	O	0.06392	0.00117	1.66872	0.02957	0.18936	0.00224	0.06025	0.00131	17	49	0.35	739	38	997	18	1118	12	1183	22	0.0
		TY62-28	S	I	N	0.06431	0.00079	1.76431	0.02111	0.19898	0.00207	0.05847	0.00060	108	109	0.99	752	26	1032	12	1170	10	1149	10	0.0
		TY62-30c	I	R	N	0.08457	0.00252	1.77789	0.05033	0.15245	0.00242	0.07665	0.00256	9	26	0.35	692	109	852	50	892	16	1056	69	0.0
		TY62-30r				0.07535	0.00153	1.31474	0.02588	0.12659	0.00164	0.04388	0.00076	69	86	0.80	658	85	741	38	756	13	759	34	0.0
Type I		TY62-32	I		N	0.06244	0.00079	0.84129	0.00947	0.09770	0.00086	0.02817	0.00026	109	99	1.10	689	27	620	11	601	9	562	9	0.0
		TY62-36c	R	S	N	0.07304	0.00120	1.62075	0.02613	0.16105	0.00190	0.04792	0.00067	74	77	0.96	1015	33	978	16	963	12	946	14	0.0
		TY62-36r				0.06568	0.00365	1.18139	0.06290	0.13059	0.00280	0.04572	0.00199	5	7	0.76	796	112	792	53	791	21	904	44	0.0
		TY62-38	R	I	N	0.06396	0.00249	1.06073	0.03951	0.12043	0.00197	0.03686	0.00102	12	10	1.10	740	80	734	37	733	16	732	28	0.0
		TY62-39	S	E	N	0.06611	0.00289	0.98475	0.04129	0.10815	0.00190	0.03364	0.00113	8	9	0.89	748	143	682	69	661	18	658	53	0.0
		TY62-50r	I	E	N	0.06735	0.00099	0.81515	0.01129	0.08782	0.00090	0.02714	0.00032	51	56	0.91	849	30	605	14	543	10	541	12	0.0
		TY62-50c				0.06414	0.00093	1.09165	0.01518	0.12347	0.00128	0.04203	0.00076	8	34	0.24	746	30	749	14	751	10	832	18	0.0
		TY62-48	R	S	N	0.07552	0.00146	1.46443	0.02739	0.14072	0.00173	0.04790	0.00083	27	35	0.76	751	77	822	35	838	13	840	32	0.0
	TY67	TY67-048	I		N	0.06297	0.00066	0.93724	0.00744	0.10813	0.00081	0.03327	0.00022	390	558	0.70	707	22	671	8	662	7	662	7	0.0
		TY67-049	R		N	0.06112	0.00068	0.82987	0.00721	0.09863	0.00075	0.02987	0.00021	494	563	0.88	643	24	614	9	606	8	595	7	0.0
		TY67-050	I		N	0.05894	0.00127	0.31577	0.00624	0.03891	0.00036	0.01159	0.00023	19	54	0.35	565	46	279	20	246	9	233	20	0.0
		TY67-051	I		N	0.06199	0.00069	0.83020	0.00712	0.09725	0.00073	0.03022	0.00022	311	433	0.72	674	24	614	9	598	8	602	7	0.0
		TY67-052	I		N	0.06259	0.00066	0.95610	0.00750	0.11089	0.00082	0.03390	0.00022	416	540	0.77	694	22	681	8	678	7	674	6	0.0
		TY67-053	I		N	0.06533	0.00119	1.13834	0.01850	0.12648	0.00115	0.04098	0.00068	24	66	0.36	785	38	772	16	768	9	812	17	0.0
		TY67-056	I		N	0.05987	0.00113	0.73082	0.01233	0.08859	0.00080	0.02790	0.00044	65	151	0.43	599	40	557	17	547	9	556	16	0.0
		TY67-057	I		N	0.05875	0.00071	0.38652	0.00370	0.04774	0.00036	0.01532	0.00012	230	370	0.62	400	47	312	20	299	8	297	13	0.0
		TY67-060	I		N	0.09587	0.00144	1.55581	0.01974	0.11772	0.00102	0.04127	0.00046	149	214	0.70	987	57	786	27	698	9	685	31	0.0
		TY67-063	I		N	0.06376	0.00076	0.90141	0.00852	0.10253	0.00078	0.03203	0.00027	62	140	0.44	734	25	652	9	629	8	637	8	0.0
		TY67-064	I		N	0.06440	0.00067	0.89928	0.00714	0.10119	0.00076	0.03189	0.00021	610	548	1.11	634	38	624	16	619	8	618	12	0.0
		TY67-065	I		N	0.06379	0.00074	0.78698	0.00738	0.08941	0.00069	0.02787	0.00022	107	117	0.92	680	41	578	18	551	8	547	13	0.0

		TY67-067	I		N	0.06335	0.00068	0.75187	0.00631	0.08602	0.00065	0.02732	0.00020	286	332	0.86	605	39	546	17	530	8	528	13	0.0
		TY67-069	I		N	0.06386	0.00065	0.75025	0.00589	0.08514	0.00064	0.02736	0.00018	514	502	1.02	548	40	531	17	523	8	522	12	0.0
		TY67-070	I		N	0.06391	0.00067	0.85786	0.00703	0.09729	0.00074	0.03056	0.00021	256	270	0.95	652	38	610	16	597	8	595	12	0.0
		TY67-071c	I	I	N	0.06384	0.00069	0.89903	0.00783	0.10207	0.00081	0.03238	0.00023	309	431	0.72	602	42	621	18	624	8	624	13	0.0
		TY67-071r				0.06379	0.00076	0.72182	0.00708	0.08201	0.00065	0.02621	0.00021	423	377	1.12	554	47	517	20	505	8	503	15	0.0
		TY67-077	I		N	0.06256	0.00072	0.77786	0.00733	0.09013	0.00071	0.02736	0.00022	156	195	0.80	693	24	584	9	556	8	546	8	0.0
		TY67-079	I		N	0.06422	0.00069	0.74777	0.00644	0.08442	0.00065	0.02652	0.00019	270	297	0.91	662	38	549	16	521	8	517	12	0.0
		TY67-082	I		N	0.06387	0.00067	0.83974	0.00692	0.09532	0.00073	0.02894	0.00020	279	294	0.95	737	22	619	8	587	8	577	7	0.0
		TY67-083	I		N	0.06302	0.00066	0.80391	0.00665	0.09251	0.00071	0.02921	0.00020	591	686	0.86	616	39	580	16	569	8	567	12	0.0
	TY16	TY16-223	R		N	0.06016	0.00723	0.15863	0.01868	0.01913	0.00050	0.00586	0.00055	7	12	0.65	609	241	150	118	122	26	118	94	0.0
		TY16-225	S		N	0.06251	0.00515	0.31757	0.02552	0.03684	0.00074	0.01330	0.00087	4	7	0.55	296	276	239	130	230	21	229	119	0.0
		TY16-226	R		N	0.06180	0.00311	0.75414	0.03632	0.08848	0.00160	0.02661	0.00136	3	7	0.51	667	104	571	48	547	18	531	51	0.0
		TY16-227c	I		N	0.06081	0.00181	0.45890	0.01297	0.05473	0.00065	0.01828	0.00037	15	18	0.74	316	118	340	53	340	12	340	36	0.0
		TY16-227r				0.05751	0.00867	0.21325	0.03142	0.02689	0.00092	0.01229	0.00115	5	9	0.60	111	532	167	264	169	36	230	144	0.0
		TY16-228	I		N	0.06161	0.00139	0.31237	0.00658	0.03677	0.00039	0.01225	0.00020	47	56	0.84	382	89	247	39	231	11	229	28	0.0
		TY16-229	R		N	0.06060	0.00157	0.47829	0.01175	0.05724	0.00065	0.01927	0.00035	26	28	0.93	267	103	347	45	355	12	356	31	0.0
		TY16-230	R		N	0.06875	0.00129	0.77830	0.01356	0.08211	0.00085	0.02574	0.00037	32	34	0.95	793	66	564	30	507	11	499	24	0.0
		TY16-026c	I		N	0.06360	0.00166	0.68019	0.01626	0.07751	0.00084	0.02428	0.00045	18	23	0.72	647	91	511	42	480	11	476	30	0.0
		TY16-026r				0.06269	0.00115	0.46910	0.00804	0.05428	0.00056	0.01829	0.00025	149	162	0.92	339	80	341	35	337	11	337	25	0.0
		TY16-028	R		N	0.06257	0.00118	0.74100	0.01317	0.08595	0.00094	0.02848	0.00051	54	99	0.54	524	69	530	30	529	11	528	30	0.0
		TY16-029	I		N	0.04977	0.00198	0.14348	0.00548	0.02092	0.00028	0.00679	0.00015	83	77	1.09	99	148	132	64	133	14	135	35	0.0
		TY16-030c	I		N	0.07829	0.00144	0.95149	0.01532	0.08809	0.00081	0.02594	0.00041	73	76	0.93	1154	36	679	16	544	9	518	16	0.0
		TY16-030r				0.05688	0.00395	0.37568	0.02505	0.04791	0.00107	0.01637	0.00076	22	25	0.90	227	251	293	115	299	23	311	73	0.0
		TY16-031c	R	S	N	0.06200	0.00256	0.64815	0.02522	0.07578	0.00114	0.02277	0.00074	8	13	0.59	674	86	507	39	471	15	455	32	0.0
		TY16-031r				0.05944	0.00471	0.28450	0.02185	0.03473	0.00076	0.01277	0.00086	7	13	0.55	146	286	214	131	217	23	222	115	0.0
		TY16-033	S		N	0.06294	0.00212	0.71843	0.02303	0.08281	0.00114	0.02708	0.00096	11	24	0.46	588	108	527	50	511	14	509	56	0.0
		TY16-034	I		N	0.06484	0.00186	1.05735	0.02894	0.11827	0.00155	0.03948	0.00108	13	22	0.56	585	95	689	43	716	13	725	42	0.0
		TY16-035	S		N	0.05438	0.00232	0.16843	0.00687	0.02247	0.00032	0.00744	0.00019	69	68	1.02	96	166	141	73	142	15	142	43	0.0
		TY16-036c	R		N	0.05404	0.00327	0.33649	0.01948	0.04513	0.00085	0.01611	0.00062	24	26	0.92	221	219	278	99	283	19	315	57	0.0
		TY16-036r				0.04682	0.00284	0.12031	0.00708	0.01863	0.00034	0.00636	0.00026	51	76	0.67	40	139	115	59	119	18	128	41	0.0
		TY16-037	I		N	0.06573	0.00579	0.17709	0.01514	0.01954	0.00045	0.00678	0.00046	12	19	0.66	450	289	143	141	123	24	121	121	0.0
		TY16-038	I		N	0.04676	0.00891	0.15541	0.02881	0.02410	0.00110	0.00993	0.00089	21	21	0.97	37	402	147	185	154	46	200	90	0.0
Type II		TY16-039	I		N	0.06699	0.01186	0.24414	0.04199	0.02643	0.00115	0.00815	0.00135	4	8	0.55	837	331	222	172	168	44	164	166	0.0
		TY16-040	I		N	0.06197	0.00125	0.95093	0.01776	0.11129	0.00112	0.03358	0.00052	28	32	0.85	673	43	679	19	680	10	668	15	0.0
	TY61	TY61-001	I		N	0.04694	0.00578	0.11852	0.01446	0.01797	0.00031	0.00407	0.00036	4	14	0.32	46	271	114	122	115	17	82	88	0.0
		TY61-002	I		N	0.22355	0.00380	2.29569	0.03306	0.07314	0.00067	0.08013	0.00079	10	22	0.43	1043	100	566	50	374	12	354	215	0.0
		TY61-003	I		N	0.05212	0.00286	0.24083	0.01292	0.03294	0.00039	0.00871	0.00034	6	19	0.33	291	121	219	54	209	12	175	39	0.0
		TY61-004	I		N	0.06009	0.00183	0.75039	0.02173	0.08909	0.00084	0.02254	0.00058	5	16	0.29	607	65	568	29	550	9	451	26	0.0
		TY61-005	I		N	0.06309	0.00177	0.97284	0.02578	0.11010	0.00102	0.02918	0.00069	4	14	0.28	711	59	690	26	673	9	581	24	0.0
		TY61-006c	I		N	0.06083	0.00189	0.95761	0.02885	0.11250	0.00125	0.02726	0.00062	10	35	0.57	633	66	682	30	687	11	544	23	0.0
		TY61-006r				0.05795	0.00224	0.42355	0.01579	0.05224	0.00054	0.01404	0.00047	5	18	0.26	528	83	359	37	328	10	282	33	0.0
		TY61-009	I		N	0.05894	0.00157	0.60436	0.01520	0.07334	0.00064	0.01665	0.00040	7	26	0.27	565	57	480	25	456	9	334	24	0.0
		TY61-010	I		N	0.06017	0.00110	0.76366	0.01258	0.09087	0.00070	0.02258	0.00030	15	47	0.32	610	39	576	16	561	8	451	13	0.0
		TY61-011	S		O	0.05023	0.00086	0.17446	0.00257	0.02522	0.00019	0.00799	0.00011	317	557	0.57	206	39	163	15	161	8	161	14	0.0
	TY61	TY61-013	R		N	0.06388	0.00127	1.00325	0.01807	0.11391	0.00104	0.03485	0.00093	5	19	0.29	738	42	705	18	695	9	692	27	0.0
		TY61-014	I		N	0.27802	0.01619	0.32543	0.01560	0.00850	0.00028	0.00341	0.00039	12	29	0.43	3194	105	262	59	53	35	44	252	0.0
		TY61-015	I		N	0.05680	0.00408	0.06202	0.00432	0.00792	0.00015	0.00250	0.00015	35	59	0.59	484	151	61	70	51	19	50	60	0.0
		TY61-016	I		N	0.05968	0.00186	0.82370	0.02399	0.10009	0.00116	0.03076	0.00137	5	19	0.27	592	66	610	29	615	12	612	45	0.0
		TY61-017	I		N	0.05956	0.00431	0.20036	0.01394	0.02440	0.00049	0.00626	0.00082	5	19	0.28	588	150	185	70	155	20	126	131	0.0
		TY61-018	I		N	0.07095	0.00654	0.17720	0.01568	0.01811	0.00047	0.00553	0.00084	5	15	0.32	956	178	166	88	116	26	111	152	0.0
		TY61-019	I		N	0.06288	0.00211	0.80470	0.02525	0.09282	0.00117	0.02855	0.00134	5	17	0.30	704	70	599	31	572	13	569	47	0.0
		TY61-020	I		N	0.05935	0.00220	0.57184	0.01991	0.06989	0.00092	0.02095	0.00091	7	19	0.38	580	79	459	35	435	13	419	43	0.0
		TY61-021	I		N	0.06368	0.00240	0.84844	0.03008	0.09667	0.00134	0.02967	0.00170	3	13	0.27	731	78	624	35	595	14	591	57	0.0
		TY61-022	I		N	0.06281	0.00148	0.79486	0.01757	0.09177	0.00099	0.02662	0.00090	5	20	0.28	702	49	594	22	566	11	531	34	0.0
		TY61-023	I		N	0.06023	0.00160	0.20818	0.00523	0.02506	0.00030	0.00793	0.00020	48	56	0.84	612	56	192	25	160	12	160	25	0.0
		TY61-027	I		N	0.05785	0.00214	0.79809	0.02821	0.10002	0.00144	0.02639	0.00127	3	9	0.35	524	79	596	35	615	14	526	48	0.0

[a] Derived from comparison of average raw counts with GJ-1 standard in each run; Ex, external; Cr, core. Shape: R, rounded; I, irregular; S, subhedral; E, euhedral; Zoning: O, oscillatory; L, lamellar; I, irregular; N, no internal structure.

sion and accuracy of the analysis, and the calculation of model ages are described in detail by Griffin et al. (2000, 2002). The results are shown in Table 3.

4. Results

4.1. Chemistry of silicate minerals

Orthopyroxene (hypersthene) contains 54.1–58.2% *En*, 39.9–44.0% *Fs* and 1.6–1.9% *Wo* in Type I xenoliths, and 57.7–61.1% *En*, 37.3–40.7% *Fs* and 1.6–2.1% *Wo* in Type II samples. Relict pyroxene identified petrographically has similar compositions to the granoblastic ones, indicating that compositional equilibrium was reached. All orthopyroxene contains significant Al_2O_3, 1.72–2.42 wt% in Type I and 2.14–2.88 wt% in Type II.

The *clinopyroxene* (Cpx) has augite to salite composition. Type I Cpx contains 43.9–45.9% *Wo*, 34.5–38.3% *En* and 17.4–21.2% *Fs*. The clinopyroxene of two garnet granulites (TY15 and TY65) contains slightly more Na_2O (∼1.04 wt%), Al_2O_3 (5.85–6.07 wt%) and TiO_2 (0.78–0.87 wt%) than the others. Type II Cpx contains 43.8–45.5% *Wo*, 35.8–37.0% *En* and 18.7–19.2% *Fs*.

Plagioclase is common in the granulite xenoliths. Granoblastic plagioclase from different samples has variable *An* contents (41–57 in Type I and 38–50 in Type II), but individual grains are homogeneous. Plagioclase within granoblastic garnet in TY65 has slightly higher *An* content (up to 62), FeO (2.45 wt%), MgO (0.36 wt%), low K_2O (0.16 wt%). High FeO and MgO may reflect the presence of submicroscopic grains of garnet. K-feldspar has a wide *Or* range (77–94%).

Olivine occurs in Type II xenoliths, and has higher FeO (33.3–35.6 wt%), MnO (0.61–0.83 wt%) and CaO (0.31–0.35 wt%), and lower $Mg^{\#}$ (0.41–0.59) than the olivine in peridotitic xenoliths (Zheng et al., 2005). *Garnet* occurs as granoblastic grains in Type I xenoliths. They are compositionally unzoned pyrope (∼47%) – almandine (∼39%) – grossular (∼12%) garnets. *Biotite*, with strong reddish brown to yellowish brown pleochroism, has 0.53 $Mg^{\#}$ and 5.92 wt% TiO_2. *Ilmenite* has wide ranges of MnO (0.07–0.91 wt%) and MgO (1.03–4.03 wt%). Ilmenite inclusions in plagioclase have lower MgO, MnO, TiO_2, but higher FeO than granoblastic grains in sample TY61. *Hematite* (as lamellae in ilmenite) in Type I samples has slightly lower TiO_2 (8.38–24.1 wt%), Al_2O_3 (1.21–2.74 wt%), MnO (0.13–0.77 wt%) and MgO (0.20–1.72 wt%) than in Type II (1.95–27.7 wt% TiO_2, 1.83–3.09 wt Al_2O_3, 0.29–1.07 wt% MnO and 0.00–2.09 wt% MgO, respectively). Hematite occurring as inclusions in plagioclase has higher MgO and FeO, and lower MnO and TiO_2 than granoblastic hematite in TY61. *Apatite* has 0.35 wt% FeO.

4.2. P–T estimates

Equilibration temperatures (Table 7) were estimated from mineral chemistry using the two-pyroxene thermometer of Wells (1977) after calculation of the Fe^{2+}/Fe^{3+} ratio, and the ilmenite–hematite thermometers of Powell and Powell (1977), Spencer and Lindsley (1981) and Andersen and Lindsley (1985) using the program of Lepage (2003). The Wells (1977) thermometer yields a rather narrow range (≈900 ± 40 °C) of equilibration temperatures. The ilmenite–hematite thermometers yield a relatively wide range of equilibration temperatures (Table 7).

For the garnet granulites, pressures of 13.5 and 13.3 kb at temperatures of 906 and 942 °C have been obtained for TY15 and TY65 using the Grt-Opx-Pl barometer (Newton and Perkins, 1982). Since the barometer was calibrated for quartz-bearing granulite assemblages and no quartz is present in the Tuoyun garnet granulites, the estimated pressure should represent an upper limit.

4.3. Major element compositions of whole rocks

Type I xenoliths vary compositionally from broadly mafic to intermediate, whereas Type II xenoliths are mafic (Table 4). The olivine granulites have slightly lower SiO_2, P_2O_5 and SiO_2/Al_2O_3, but higher TiO_2, Al_2O_3 and Na_2O than the quartz granulites. All samples are olivine-normative (0.39–15.5%) except TY13 and TY1b, and contain variable normative calcite (0.23–1.14%), apatite (0.07–0.97%) and ilmenite (1.61–3.17%). TY13 and TY1b are quartz-normative. TY61 (pyroxene granulite) and TY12 (olivine granulite), among the Type II samples, have 2.76 and 6.97% normative nepheline, respectively.

Except for TY67 and TY1b (Type I) and TY61 and TY12 (Type II), the Tuoyun granulitic xenoliths plot on the boundary between alkaline and sub-alkaline rocks (Fig. 2a). TY67 and TY1b are sub-alkaline, while TY61 and TY12 are alkaline rocks. Type I samples are mainly calc-alkaline, with a few low-potassium tholeittic-series rocks (Fig. 2b), while Type II xenoliths range from the low-potassium tholeittic to alkalic series. The SiO_2 content of the Tuoyun xenoliths, especially those from Type II, shows negative correlations with MgO and CaO, broadly negative correlation with TiO_2, and broadly positive correlation with Na_2O, but no correlation with Al_2O_3 (Fig. 3) and K_2O (see Fig. 2b).

Table 7
Estimated equilibration temperature (T), pressure (P) and oxygen fugacity ($\log_{10}fO_2$)

Type	Sample	T_{W77} (°C)[a]	P_{NP82} (kb)	T_{PP77} (°C)	T_{SL81} (°C)	$\log_{10}fO_2$	T_{AL85} (°C)	$\log_{10}fO_2$
Type I	TY13	872		841	728	−17.5	750	−17.1
	TY62	885		889	866	−13.2	855	−13.5
	TY67	871		835	832	−11.9	830	−12.4
	TY1b	875		866	727	−17.7	752	−17.4
	TY7d	878		790	511	−26.3	545	−25.8
	TY15	906	13.5					
	TY65	942	13.3					
Type II	TY16	919						
	TY17	941						
	TY61	871		899	638	−21.2	670	−20.9
	TY61 (Inc.)			770	584	−22.7	624	−21.7
	TY12	858		930	928	−12.0	898	−12.6

[a] Temperature calculation under $P = 10$ kb; inc., Ilmenite with hematite lamellae inclusion in plagioclase; T_{W77}, thermometer of Wells (1977); P_{NP82}, Grt-Opx-Pl barometer of Newton and Perkins (1982); T_{PP77}, thermometer of Powell and Powell (1977).

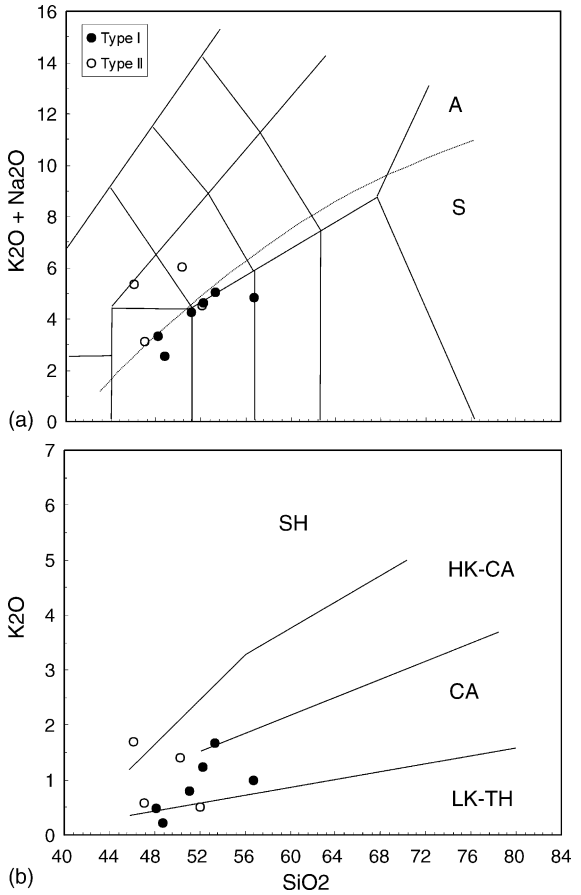

Fig. 2. TAS (a) and SiO_2–K_2O (b) plots of the Tuoyun granulites. (a) After Le Bas et al. (1986); the boundary between alkaline (A) and subalkaline (S) series is from Irvine and Baragar (1971). (b) LK-TH, low-potassium tholeittic; CA, calc-alkalic; HK-CA, high-potassium calc-alkalic.

4.4. Trace element compositions of whole rocks

Type I xenoliths have high REE contents, and LREE-enriched patterns with wide ranges in $(La/Yb)_n$ (1.83–12.1) and δEu (defined as $2(Eu)_N/((Sm)_N + (Gd)_N)$, 0.79–1.24). Garnet granulite TY15 has the lowest $(La/Yb)_n$ (1.83). Type II samples also have high REE contents (59.0–163 ppm) and LREE-enriched patterns but with relatively narrow ranges of $(La/Yb)_n$ (2.60–8.48) and δEu (1.00–1.19).

All Tuoyun granulite xenoliths have low Th/U, Th/La and Ce/Pb, and are depleted in Th relative to REE. However, they have higher K/Rb and Ba/La than the primitive mantle (McDonough and Sun, 1995), and are highly enriched in Sr and Ba. The Type I xenoliths have slightly lower Ni, Cr, Th/U, Th/La, Nb/Y, Ce/Pb, higher Sc, Ba/La and La/Nb than the Type II xenoliths. Type I has marked negative anomalies in Zr, Hf, Ti, Nb and Ta (Fig. 4a), whereas Type II has no, or very weak, Zr and Hf anomalies (Fig. 4b). Nearly half of the Type II samples have negative Ti, Nb and Ta anomalies; the rest have no Ti anomaly and positive Nb and Ta anomalies. $Mg^{\#}$ is positively correlated with Ni, V and Sc in Type I samples, but poorly correlated in Type II xenoliths (Fig. 5).

4.5. Zircon morphology and internal structure

Backscattered electron/cathodoluminescence (BSE/CL) imaging provides essential information on the external and internal structure of single zircon grains, which is especially important in revealing their multi-stage history. BSE/CL images were taken of 142 grains from four granulite xenoliths. Their external forms have

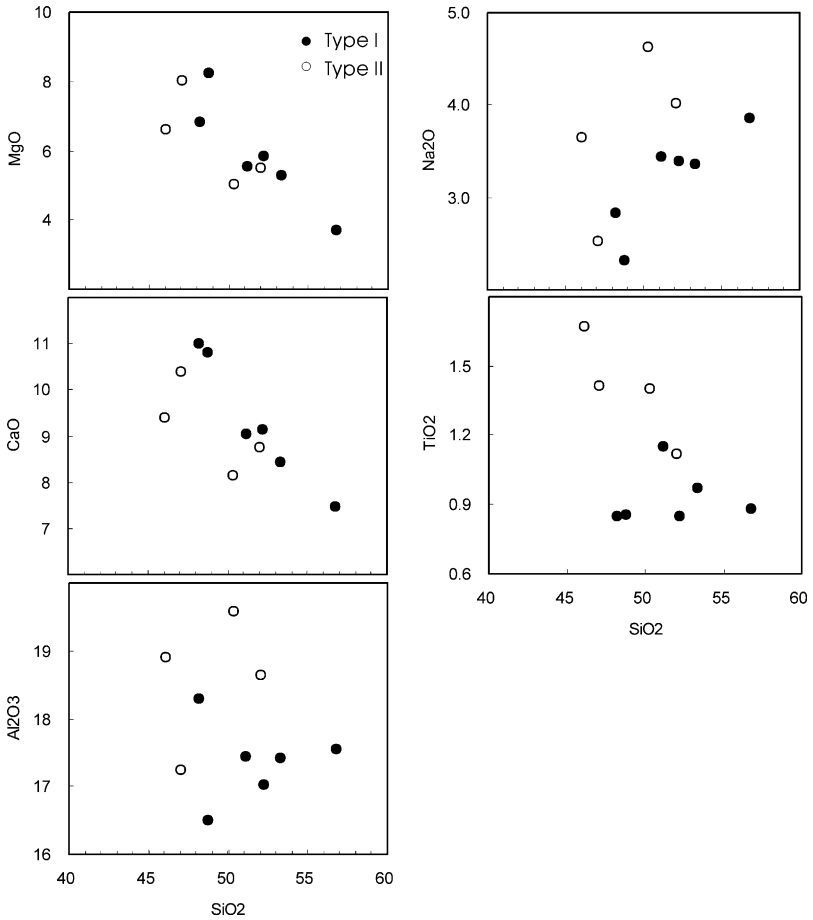

Fig. 3. Plots of SiO_2 against other oxides in the Tuoyun granulite xenoliths.

been classified (Table 3) as euhedral, subhedral, rounded or irregular. The BSE/CL images reveal the presence of distinct cores in ca. 30% of the grains, recognized by different zoning patterns, or as bright zones with rounded or irregular shapes, surrounded by unzoned rims. Internal zoning structures of cores and rim areas have been divided into oscillatory, lamellar or irregular; many grains show no internal structure (Fig. 6; Tables 3 and 6).

4.6. U–Pb dating of zircons

4.6.1. Type I granulites

Zircons from TY62 are dark purple, transparent and generally euhedral–subhedral in external form (50–200 μm). The BSE/CL images show that many of the grains contain euhedral to rounded cores, surrounded by structureless rims. The obvious cores in some grains have high BSE/CL brightness, but are not clearly zoned. Thirty-three zircon grains were analyzed in 40 points. The results show a broad scatter of $^{206}Pb/^{238}U$ ages, respectively, ranging from 319 to 1170 Ma with multiple peaks (Fig. 7). However, some grains with $^{206}Pb/^{238}U$ ages >900 Ma are reversely discordant, suggesting metamorphic disturbance of their U–Th–Pb systematics, and these have been rejected from further consideration. Cores and rims were analysed separately in seven grains; the difference in age is significant at the two-sigma level in most cases, with the rims being 10–108 Ma younger ($^{206}Pb/^{238}U$ ages). Thirty-six points lie along Concordia between 850 and 550 Ma, and the data are interpreted as reflecting quasi-continuous Pb loss over a period of ca. 150 Ma.

Zircons from TY67 are light purple, transparent, mainly irregular in external form (80–140 μm) and lack internal structure. Twenty zircon grains were analyzed in 21 points. The U–Pb data show a broad scatter of $^{206}Pb/^{238}U$ ages ranging from 246 to 768 Ma with a peak at 600 Ma. Core and rim were analysed separately in one grain (TY67-071), the rim is 119 Ma younger ($^{206}Pb/^{238}U$ ages). Nineteen points define a discordia

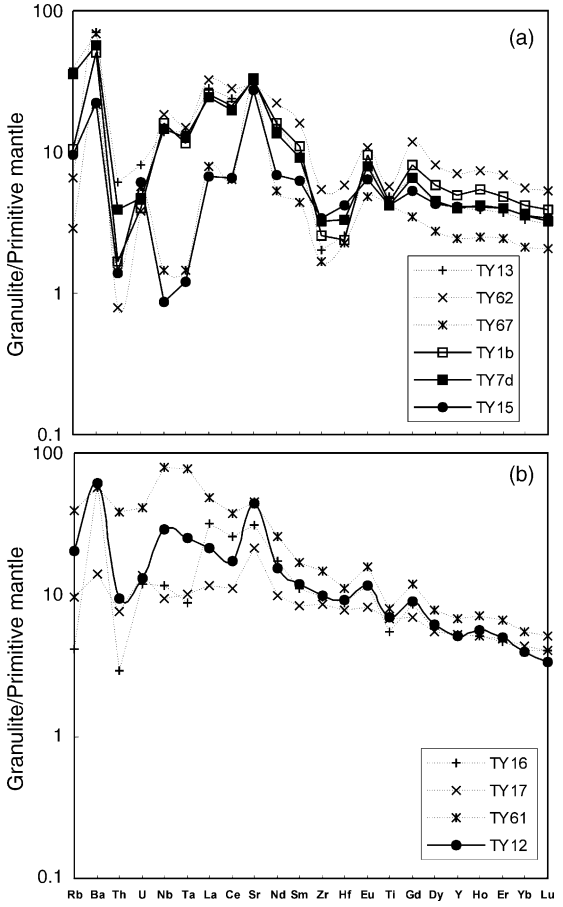

Fig. 4. Spidergrams for the Tuoyun granulite xenoliths (a) Type I and (b) Type II.

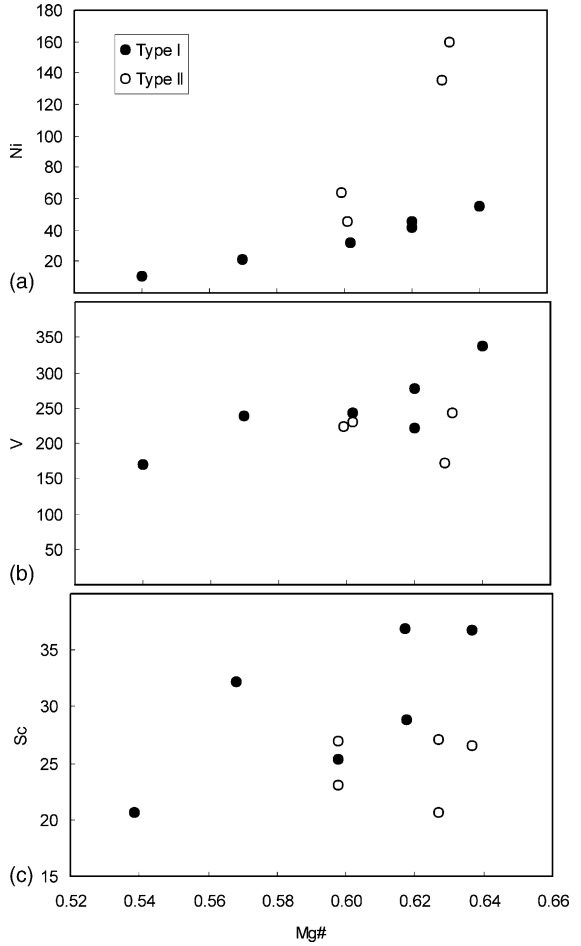

Fig. 5. Plots of $Mg^{\#}$ against Ni (a), V (b) and Sc (c) for the Tuoyun granulite xenoliths.

with an upper intercept age of 767 ± 23 Ma and a lower intercept age of 123 ± 44 Ma.

4.6.2. Type II granulites

Zircons from TY16 are light purple, transparent and generally subhedral-irregular in external form (90–130 μm) without internal structure. Twenty zircon grains were analyzed in 25 points (Table 6). The U–Pb data show a broad scatter of non-concordant $^{206}Pb/^{238}U$ ages from 118 to 725 Ma with several peaks. Cores and rims were analysed separately in five grains; the differences in age are significant at the two-sigma level, the rims being younger by 143–254 Ma ($^{206}Pb/^{238}U$ ages). Twenty-two points define a discordia with an upper intercept age of 721 ± 47 Ma and a lower intercept age of 81 ± 40 Ma.

Zircons from TY61 are purple, transparent and mainly irregular to round in external form (80–200 μm), and lack any internal structure. Twenty-one grains were analyzed in 22 points. The U–Pb data show a broad scatter of non-concordant $^{206}Pb/^{238}U$ ages ranging from 51 to 695 Ma with several peaks. Cores and rims were analysed separately in one grain (TY61-006); the difference in age is significant at the two-sigma level, the rim being 105 Ma younger. Seventeen points define a discordia with an upper intercept age of 707 ± 36 Ma and a lower intercept age of 116 ± 49 Ma.

4.7. Hf-isotope compositions of zircons (Table 3)

The Hf-isotope ratios are plotted against U/Pb age in Fig. 8a. The uniformity of the Hf-isotope ratios over wide age ranges strongly suggests that most of the younger zircons reflect recrystallisation of the older population, without modification of the Hf-isotope ratios. The ε_{Hf} of zircon grains with identical $^{176}Hf/^{177}Hf$, but different ages, will become progressively lower with decreasing age (Fig. 8b). If the populations are related by simple Pb loss, they will fall along a simple trajectory, as is

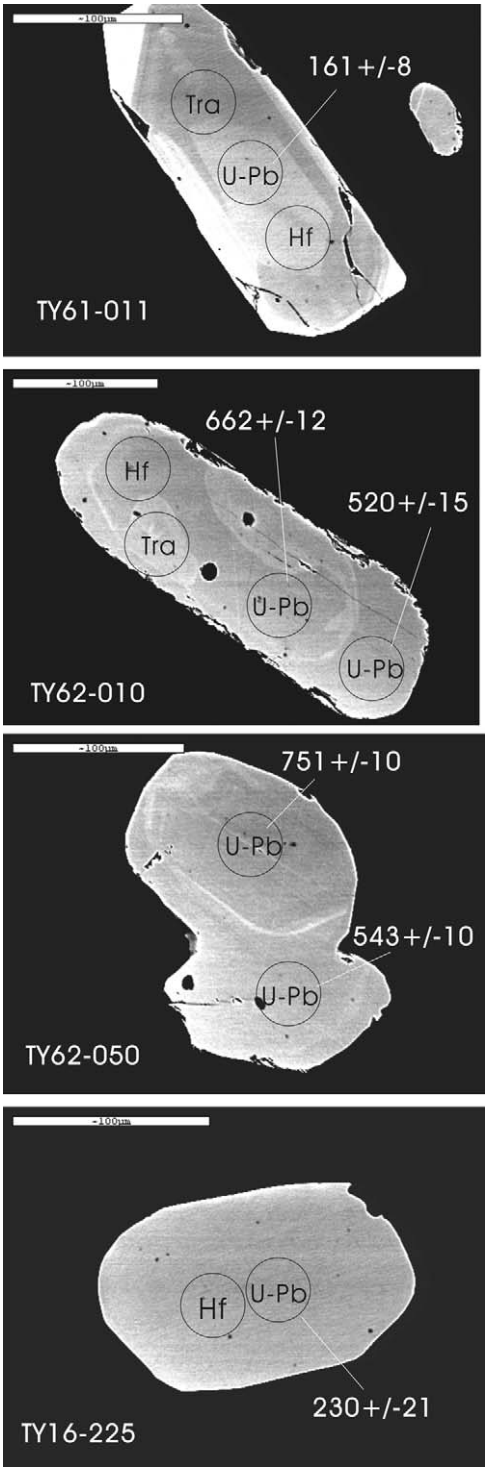

Fig. 6. BSE/CL images showing zircon morphology, internal structure and typical positions for in situ analyses of age (U–Pb), Hf-isotopes (Hf) and trace element contents (Tra).

illustrated by the data from these samples. If a younger population lies above the Pb-loss trajectory of an older one from the same sample, this implies that the younger population represents the growth of new zircon, which incorporated radiogenic ^{176}Hf that grew in during the time interval between the two populations. All but one of the analysed zircons from TY61 lie close to such Pb-loss trajectories, suggesting that the "ages" of zircons in Tuoyun granulites may reflect Pb loss related to recrystallisation. Grain TY61-011, a euhedral zircon, lies above the Pb-loss trajectory formed by the older grains in TY61. We interpret this younger grain as having grown at 116 Ma from Zr (and Hf) liberated from older silicates or oxides with relatively high Lu/Hf and ^{176}Lu/^{177}Hf. This is consistent with its euhedral external form (see Fig. 3a).

The minimum depleted-mantle model ages (Table 3) for the zircons cluster around 1.5–1.65 Ga, indicating that the ca. 800 Ma mafic rocks contain a significant component of Hf derived from older crustal rocks. If the crustal component is assumed to have the ^{176}Lu/^{177}Hf of the average continental crust (0.015), the least radiogenic Hf in these zircons at ca. 800 Ma requires a minimum age of ca. 2.3 Ga.

5. Discussion

5.1. Lithospheric thermal state of northwestern Tianshan

Other lower crustal xenoliths in the East Central Asia Orogenic Belt (Stosch et al., 1995) have been reported from the Tariat region (in central Mongolia) and the Dariganga Plateau (in southeastern Mongolia) in Oligocene alkali basalts (Khutorskoy and Yarmolyuk, 1989). Garnet-bearing deep-seated xenoliths including granulite, pyroxenite and peridotite in the Tariat region appear to follow model geotherms corresponding to heat flow of 70–80 mW/m^2 in a crust about 50 km thick (Ryabchibov et al., 1983; Stosch et al., 1995). The Tuoyun granulite xenoliths have higher equilibration temperatures than the Tariat granulites (907 ± 35 °C versus 840 ± 30 °C) using the Wells (1977) thermometer. However, equilibration pressures of Tuoyun garnet granulites are low relative to those from Tariat (≤13.4 ± 0.1 kb versus 14 ± 1.5 kb) using the Grt-Opx-Pl barometers of Newton and Perkins (1982), suggesting an even higher geotherm (~90 mW/m^2) beneath the Tuoyun basin at the time the host-magma erupted (Fig. 9). The temperature estimates for the Tuoyun granulites coincide with the lower limit of the temperature range (932–1004 °C, Zheng et al., 2005) obtained for

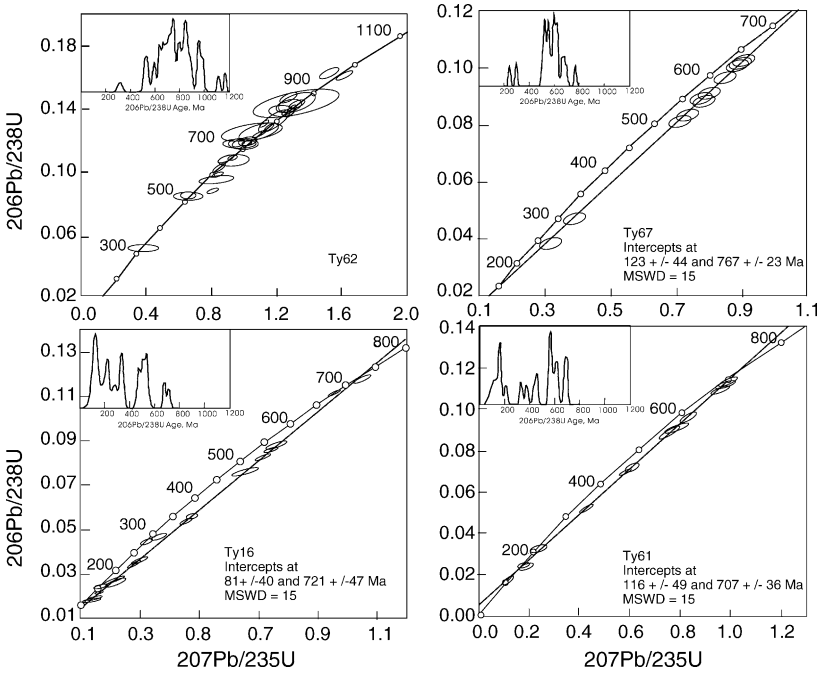

Fig. 7. Inverse-Concordia plots of U–Pb isotopic results.

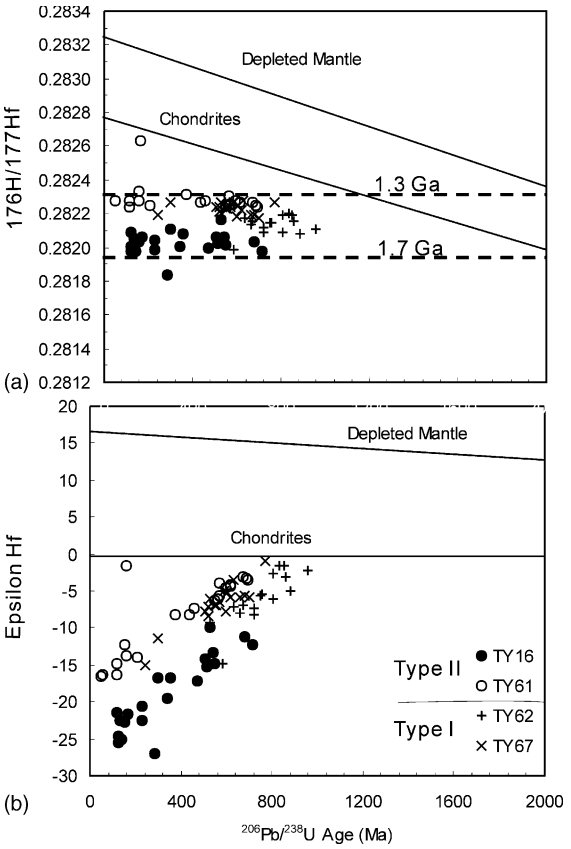

Fig. 8. $^{206}Pb/^{238}U$ age vs. Hf-isotope composition (a) and ε_{Hf} (b) for zircons from the Tuoyun granulites.

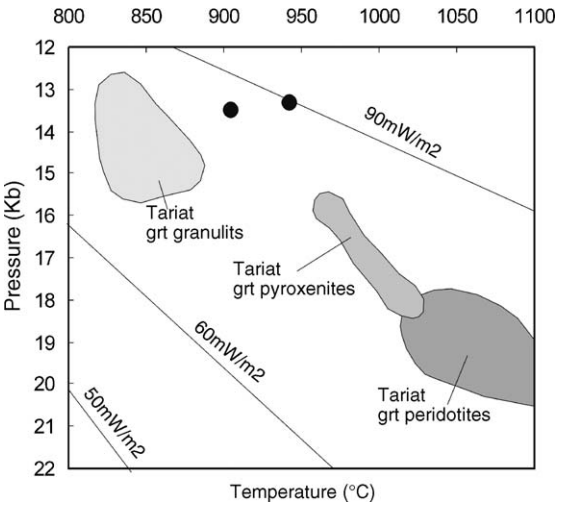

Fig. 9. *P–T* plot showing garnet granulite xenoliths from the Tuoyun and Tariat regions. Tariat data for garnet-bearing granulites are from Stosch et al. (1995) and Kopylova et al. (1995); garnet-bearing pyroxenites and peridotites are from Ryabchibov et al. (1983) and Kopylova et al. (1995). *T* calculated using the Wells (1977) geothermometer, *P* using the Grt-Opx-Pl barometer of Newton and Perkins (1982) for the granulites and of Nickel and Green (1985) for pyroxenite and peridotite xenoliths. Three model conductive geotherms for continental regions, adopted from Pollack and Chapman (1977), are plotted for comparison.

spinel peridotite xenoliths in the same basaltic flow using the same method (Wells, 1977), suggesting that the granulites were derived from near the crust–mantle boundary.

5.2. Petrogenesis of Tuoyun granulite xenoliths

Many processes have been suggested for the origin of mafic lower crustal xenoliths, such as residues of partial melting, cumulates and metamorphic mineral segregation (Rudnick, 1995) and metasediments (Stosch et al., 1989). We consider the Tuoyun granulites to be meta-igneous xenoliths, mainly based on the typically magmatic cores preserved in zircons in all four Tuoyun granulite xenoliths (especially in TY62; see Table 6), and the preservation of apparently magmatic olivine and pyroxene in some Type II xenoliths.

CaO and MgO define clear trends when plotted against SiO_2 (see Fig. 3), further suggesting that the Tuoyun granulites are primarily the products of magmatic crystallization. Good positive correlations of $Mg^{\#}$ against Ni, Cr and Sc in the Type I (see Fig. 5) imply that olivine and pyroxene (especially the former) are the main phases involved in fractional crystallization during their petrogenesis. Positive (δEu = 1.24 in TY67) and negative (δEu = 0.79 in TY62) Eu anomalies indicate that both accumulation and fractionation of plagioclase occurred. The broad negative correlation between SiO_2 and TiO_2 implies that fractional crystallization of ilmenite also occurred. However, the broad scatter in plots of SiO_2 against Na_2O, K_2O and especially against Al_2O_3 (see Figs. 2 and 3) suggest that contamination by felsic crustal components may also have occurred. This is supported by the wide ranges in incompatible trace elements, and the wide ranges of La/Nb, Nb/Y, Nb/U, Ta/U and Ce/Pb (see Table 5).

5.3. Formation and evolution of the lower crust, southwestern Tianshan

The U–Pb and Hf-isotopes presented above suggest that the Tuoyun granulite xenoliths of both Types I and II have undergone protracted cooling and recrystallisation in the lower crust. The data from sample Ty62 suggest a long period of cooling and continuous Pb loss, while the upper intercepts of the discordia for the other samples suggest igneous crystallization ages ranging from 760 to 700 Ma. Most of the zircon populations have experienced episodic Pb loss at 80–125 Ma, corresponding roughly to the eruption ages of the lavas.

All the zircons in the Tuoyun xenoliths have ε_{Hf} significantly below zero, indicating that they contain Hf that was separated from the depleted mantle at some time well before 750 Ma. The T_{DM} model ages of the zircons (calculated using the measured Lu/Hf) cluster in the range 1.3–1.7 Ga (Table 3); these model ages must represent minimum ages for this event. One interpretation of these data is that the protoliths of the granulites actually were intruded at this time, and that the upper intercept ages represent the timing of granulite facies metamorphism. This interpretation would require that the zoning observed in the cores of ca. 30% of the grains is relict after the magmatic event, and has survived the complete resetting of the U–Pb systems. However, the upper intercept ages (690–770 Ma) and the ages of the oldest concordant zircons from the Tuoyun granulite xenoliths (750–900 Ma), coincide with a widespread Neoproterozoic crustal generation event, marked by zircon U–Pb ages (707–882 Ma) of the granitic-tonalitic-granodioritic gneisses (Chen, 1999; Chen et al., 2000). This coincidence supports a magmatic interpretation of the upper-intercept ages.

The Sr–Nd isotopes and trace elemental compositions of the host-rocks with the oceanic Island basaltic affinity (Sobel and Arnaud, 2000; Wang et al., 2000) and their peridotite xneoliths with ‘oceanic’ affinity (Zheng et al., 2005) suggest that the Neoproterozoic mafic magmas (the protolith of the granulite xenoliths) could not be derived from the melting of a long-term metasomatized lithosheric mantle. On the other hand, the Tianshan is a complex Paleozoic orogen with composite terrains (e.g. Windley et al., 1990; Xiao et al., 1992; Gao et al., 1995, 1998; Hu et al., 2000; Gao and Klemd, 2003). The lower crust and lithosphere of the Tarim plate were partly subducted during the collisions (Hendrix et al., 1994; Poupinet et al., 2002), and Neoproterozoic blueschists and greenschists are exposed in northwestern Tarim (Nakajima, 1990; Xiao et al., 1992), adjacent to the southern Tianshan region. Therefore, two mechanisms for the formation of the granulites should be considered: (1) the granulites were formed along an active continental margin of the Yini-Central Tianshan plate in Neoproterozoic (690–770 Ma) and were thrust to upper levels of the crust during Paleozoic-Mesozoic time; (2) the protoliths of the granulite xenoliths formed during Neo-Proterozoic time in the northwestern Tarim plate and were subducted to the lower crust level in Late-Cretaceous as a result of collision between the Tarim and Yini-Central Tianshan plates.

However, the temperature estimates for the Tuoyun granulites coincide with the lower limit of the temperature range for spinel peridotite xenoliths from the same flow (Zheng et al., 2005), suggesting that the lower crust and upper mantle were coupled. Furthermore, the oscillatory zoning of zircon cores is accompanied by

very low $\varepsilon_{Hf,}$ which requires the addition of an older crustal component. These observations suggest that the most probable interpretation of the granulites is that they represent underplated basaltic magmas, which assimilated pre-existing crustal components at the base of the crust.

If the upper-intercept ages are accepted as approximating the time of intrusion of the magmatic precursors to the mafic granulites, then they must have assimilated large amounts of Hf from significantly older crustal rocks. The age of this older crust, and the degree of contamination, cannot be unambiguously calculated. However, one constraint can be provided by assuming that the crustal rocks had the $^{176}Lu/^{177}Hf$ of the average continental crust (0.015; Griffin et al., 2000; Table 3). If we assume that the Hf-isotope compositions of the mafic-intermediate magmas represent mixing between this continental crust and a depleted-mantle component at ca. 850–900 Ma (the age of the oldest concordant zircons), we can calculate the model age of the crustal component required for different degrees of assimilation. If >90% of the Hf in the mafic granulites is crustal, the average source rocks would be 2.5–2.8 Ga old; if 50% of the Hf is crustal, the average source rocks would be ca. 3.4 Ga old; if only 25% assimilation is allowed, the model age of the crustal component becomes ca. 4 Ga. There is some evidence in the Hf-isotope and whole-rock chemistry that such assimilation may have occurred, such as the broad scatter in plots of SiO_2 against Na_2O, K_2O and Al_2O_3. There is a good negative correlation in the four dated samples between mean $^{176}Hf/^{177}Hf$ and SiO_2 content; the least radiogenic (most contaminated) sample has 52% SiO_2 (TY16) and the most radiogenic (least contaminated) sample has 46% SiO_2 (TY61). Assimilation may also be recorded by some highly disturbed, but apparently older (inherited), zircons in TY62 (Table 6).

The oldest depleted-mantle Hf model ages calculated for 700–800 Ma zircons, and assuming an average crustal Lu/Hf (T^c_{DM}, 1.97–1.8 Ga, see Table 3) are similar to, but younger than, the Nd model ages (2.2–1.2 Ga) of exposed amphibolite and granitic gneisses (Hu et al., 1997, 2000). However, the Hf-isotope data require that the crustal rocks that were assimilated by the lower-crustal mafic granulites must be significantly older than these exposed surface rocks. This is similar to the situation recently documented in the southern part of the North China Craton, where lower-crustal granulites give U–Pb zircon ages >3.6 Ga (Zheng et al., 2004), although the oldest exposed rocks are ca. 2.85 Ga. Therefore, we suggest that the original lower crust beneath the Tuoyun area formed during Mesoarchean to Paleoarchean time, and represents a relict Archean microcontinental block in the southwestern Tianshan. This lower crust experienced Neoproterozoic (700–850 Ma) underplating and reworking by mafic magmas, simultaneously with the formation of granitic gneisses in the middle crust.

The lower intercept ages and some younger near-concordant ages (123–82 and 51–60 Ma) of zircons in Tuoyun granulites are similar to the eruption ages (120–110 and 67–46 Ma) of their host basalts (Li et al., 1995; Wang et al., 2000; Liang et al., 2005), and may reflect heating by a small "plume" (Sobel and Arnaud, 2000), which appears on seismic tomography beneath the Tuoyun region (Xu et al., 1998, 2000). Therefore, we interpret this thermal event, with its high geotherm of ~90 mW/m^2, as resulting from asthenospheric upwelling during late Mesozoic to Paleogene, which resulted in episodic Pb-loss from the zircons in the lower crust.

6. Conclusions

1 A granulite xenolith suite from the Mesozoic–Cenozoic Tuoyun basatic rocks of Xinjiang Province (NW China) includes foliated and massive mafic rocks with clear magmatic characteristics (reflecting fractional crystallization and accumulation), but some evidence for the assimilation of more felsic crustal rocks. The crustal thickness of the Tianshan region in Cretaceous-Paleogene time reached ca. 40 km with a geotherm of ~90 mW/m^2.

2 The upper intercept ages of 690–770 Ma, and concordant zircons as old as 850–900 Ma, are interpreted as the age of magmatic underplating and subsequent granulite-facies metamorphism, during a recognized major period of crustal formation in the southwestern Tianshan region. The lower intercept ages of 80–125 Ma, and some younger concordant zircons down to 50 Ma, reflect a major thermal event in the lower crust, related to the eruption of the host basalts, which resulted in Pb-loss from the zircons.

3 The mean Hf model ages (T_{DM}) of the zircons in the four samples range from 1.3 to 1.7 Ga. If the upper intercept ages are interpreted as magmatic, these represent minimum ages for intrusion of the mafic magmas. If their magmatic ages are 750–850 Ma, at least 50% the Hf in the zircons was derived by assimilation of pre-existing crustal rocks. Assuming this older crust to have the Lu/Hf ratio of average continental crust requires that the lower crust beneath the southwestern Tianshan (e.g. in Tuoyun area) was at least Neoarchean (>2.5 Ga), and probably Mesoarchean (3.4 Ga) in Neoproterozoic time. This is significantly

older than known upper crust in the southwestern Tianshan region.

Acknowledgments

We thank Dr. Elena Belousova, and Suzy Elhlou and Carol Lawson, for their constant and patient assistance with the analytical work. Drs. Z.H. Luo and J. Gao are thanked for their constructive instruction and help. The first author would like to thank Dr. R.Y. Zhang for their discussion during his visit to Stanford in 2003–2004. Two anonymous reviewers are thanked for their constructive comments and suggestions. This study was supported by the Chinese Natural Science Funding (40273001 and 40425002), PCSIRT (IRT0441), the ACILP AusAID Program and an ARC Discovery Project grant (SYO'R and W.L.G.). This is contribution no. 421 from the ARC National Key Centre for the Geochemical Evolution and Metallogeny of Continents (www.els.mq.edu.au/GEMOC/).

References

Allen, M.B., Windley, B.F., Zhang, G., 1992. Paleozoic collisional tectonics and magmatism of the Chinese Tianshan, central Asia. Tectonophysics 220, 89–115.

Allen, M.B., Windley, B.F., Zhang, G., Zhao, Z., Wang, G., 1991. Basin evolution within and adjacent to the Tianshan Range NW China. J. Geol. Soc. Lond. 148, 369–378.

Andersen, D.J., Lindsley, D.H., 1985. New models for the Ti-magnetite/ilmenite geothermometer and oxygen barometer. In: Spring Meeting, American Geophysical Union, vol. 66, no. 18, p. 416.

Andersen, T., 2002. Correction of common lead in U–Pb analyses that do not report ^{204}Pb. Chem. Geol. 192, 59–72.

Belousova, E.A., Griffin, W.L., Shee, S.R., Jackson, S.E., O'Reilly, S.Y., 2001. Two age populations of zircons from the Timber Creek kimberlites, Northern territory Australia as determined by laser ablation ICPMS analysis. Aust. J. Earth Sci. 48, 756–766.

Blichert-Toft, J., Albarede, F., 1998. The Lu–Hf geochemistry of chondrites and evolution of the mantle–crust system. Earth Planet Sci. Lett. 148, 243–258.

Brookfield, M.E., 2000. Geological development and Phanerozoic crustal accretion in the western segment of the southern Tianshan (Kyrggzstan Uzbokistan and Tajikstan). Tectonophysics 328, 1–14.

Carroll, A.R., Graham, S.A., Hendrix, M.S., Ying, D., Zhou, D., 1995. Late Paleozoic tectonic amalgamation of northwestern China: sedimentary record of the north Tarim, northwestern Turpan and southern Junggar basins. Geol. Soc. Am. Bull. 107, 571–594.

Chen, B., Jahn, B.M., 2004. Genesis of post-collisional granitoids and basement nature of the Junggar Terrane NW China: Nd–Sr isotope and trace element evidence. J. Asian Earth Sci. 23, 691–703.

Chen, C.M., Lu, H.F., Jia, D., Cai, D.S., Wu, s.Mi, 1999. Closing history of the southern Tianshan oceanic basin, western China: an oblique collisional orogeny. Tectonophysics 302, 23–40.

Chen, J., Burbank, D.W., Scharer, K.M., Sobel, E., Yin, J.H., Rubi, C., Zhao, R.B., 2002. Magneto-chronology of the Upper Cenozoic strata in the Southwestern Chinese Tianshan: rates of Pleistocene folding and thrusting. Earth Planet. Sci. Lett. 195, 113–130.

Chen, Y.B., 1999. Isotope geochemistry study on the basement of the western Tianshan, Xinjiang, Northwestern China. Ph.D. Dissertation. Guangzhou Institute of Geochemistry, Chinese Academy of Sciences, 51 pp.

Chen, Y.B., Hu, A.Q., Zhang, G.X., Zhang, Q.F., 2000. Zircon U–Pb age of granitic gneiss on Duku highway in western Tianshan of China and its geological implications. Chin. Sci. Bull. 45, 649–653.

Coleman, R.G., 1989. Continental growth of north China. Tectonics 8, 621–636.

Condie, K.C., 1999. Mafic crustal xenoliths and the origin of the lower continental crust. Lithos 46, 95–101.

Debievre, P., Taylor, P.D.P., 1993. Table of the isotopic composition of the elements. Int. J. Mass Spectrum (Ion Process) 123, 149.

Fu, Z.X., 2000. The large-scale distribution of great shallow intraplate earthquakes in mainland China and adjacent areas and seismic coupling along plate margins. J. Asian Earth Sci. 18, 41–46.

Gao, J., He, G., Li, M., Xiao, X., Tang, Y., Wang, J., Zhao, M., 1995. The mineralogy, petrology, metamorphic PTDt trajectory and exhumation mechanism of blueschists, southern Tianshan, northwest China. Tectonophysics 250, 151–168.

Gao, J., Klemd, R., 2003. Formation of HP-LT rocks and their tectonic implications in the western Tianshan Orogen NW China: geochemical and age constraints. Lithos 66, 1–22.

Gao, J., Li, M.S., Xiao, X.C., Tang, Y.Q., He, G.Q., 1998. Paleozoic tectonic evolution of the Tianshan Orogen NW China. Tectonophysics 287, 213–231.

Graham, S.A., Brassell, S., Carroll, A.R., Xiao, X., Demaison, G., Mcknight, C.L., Liang, Y., Chu, J., Hendrix, M.S., 1990. Characteristics of selected petroleum source rocks, Xinjiang Uygar autonomous region, northwest China. Am. Assoc. Pet. Geol. Bull. 74, 493–512.

Griffin, W.L., O'Reilly, S.Y., 1986. The lower crust in eastern Australia: xenolith evidence. In: Dawson, J.B., Carswell, D.A., Hall, J., Wedepohl (Eds.), Nature of the Lower Crust. Geol. Soc. Sep. Pub. No. 24, London, pp. 363–374.

Griffin, W.L., Pearson, N.J., Belousova, E., Jackson, S.E., O'Reilly, S.Y., van Achterberg, E., Shee, S.R., 2000. The Hf isotope composition of cratonic mantle: LAM-MC-ICPMS analysis of zircon megacrysts in kimberlites. Geochim. Cosmochim. Acta 64, 133–147.

Griffin, W.L., Wang, X., Jackson, S.E., Pearson, N.J., O'Reilly, S.Y., Xu, X.S., Zhou, X.M., 2002. Zircon chemistry and magma mixing: SE China: in situ analysis of Hf isotopes. Tonglu and Pingtan igneous complex. Lithos 61, 237–269.

Han, B.F., Wang, X.C., He, G.Q., 1998. Discovery of upper mantle and lower crust xenolith in early Cretaceous volcanic rock from southwest Tianshan. Chin. Sci. Bull. 43, 2544–2547 (in Chinese).

Hendrix, M.S., Dumitru, T.A., Graham, S.A., 1994. Late Oligocene-early Miocene un-roofing in the Chinese Tianshan: an early effect of the India-Asia collision. Geology 22, 487–490.

Hirata, T., Nesbitt, R.W., 1995. U–Pb isotope geochronology of zircon: evaluation of the laser probe-inductively coupled plasma-mass spectrometry technique. Geochim. Cosmochim. Acta 59, 2491–2500.

Hu, A.Q., Jahn, B.M., Zhang, G.X., Chen, Y.B., Zhang, Q.F., 2000. Crustal evolution and Phanerozoic crustal growth in northern Xinjiang: Nd isotopic evidence. Part I. Isotopic characterization of basement rocks. Tectonophysics 328, 15–51.

Hu, A.Q., Wang, Z.G., Tu, G.Z., 1997. Geological Evolution and Diagenic and Metallogenetic Regularity in Northern Xinjiang. Science Press, Beijing, pp. 9–105 (in Chinese).

Irvine, T.N., Baragar, W.R.A., 1971. A guide to the chemical classification of the common volcanic rocks. Can. J. Earth Sci. 8, 523–548.

Jackson, S.E., Pearson, N.J., Griffin, W.L., Belousova, E.A., 2004. The application of laser ablation-inductively coupled plasma-mass spectrometry to in situ U–Pb zircon geochronology. Chem. Geol. 211, 47–69.

Khutorskoy, M.D., Yarmolyuk, V.V., 1989. Thermal and magmatic evolution of the lithosphere of Mongolia. Int. Geol. Rev. 31, 1084–1096.

Kopylova, M.G., O'Reilly, S.Y., Genshaft, Y.S., 1995. Thermal state of the lithosphere beneath Central Mongolia: evidence from deep-seated xenoliths from the Shavaryn-Saram volcanic center in the Tariat depression, Hangai, Mongolia. Lithos 36, 243–255.

Le Bas, M., Le Maitre, R.W., Streckeisen, A., Zanettin, B., 1986. A chemical classification of volcanic rocks based on the total-silica diagram. J. Petrol. 27, 745–750.

Lepage, L.D., 2003. ILMAT: an Excel worksheet for ilmenite-magnetite geothermometry and geobarometry. Comput. Geosci. 29, 673–678.

Li, Y.A., Li, Q., Zhang, H., 1995. Paleo-magnetic study and implication on formation and evolution of Tarim basin. Xinjiang Geol. 13, 293–376 (in Chinese).

Liang, T., Luo, Z.H., Li, W.T., Ke, S., Li, L., Zhan, H.M., 2005. Geologic features and tectonic implications of the Tuoyun volcano group. Xinjiang Geol. 23, 105–110 (in Chinese).

Lin, S.L., He, M., Hu, S.H., 2000. Precise determination of trace elements in geological samples by ICPMS using compromise conditions and fine matrix-matching strategy. Anal. Sci. 16, 1290–1296.

Ludwig, K.R., 2000. Isoplot—A Geochronological Toolkit for Microsoft Excel. Berkeley Geochronology Center. Spec. Pub. No. 1a, p. 53.

McDonough, W.F., Sun, S.S., 1995. The composition of the Earth. Chem. Geol. 120, 223–253.

Nakajima, T., 1990. Evidence for early Proterozoic plate tectonics from reflection profiles in Baltic Shield. Nature 346, 263–265.

Nelson, M.R., Mccafferey, R., Molnar, P., 1987. Source parameters for eleven earthquakes in the Tianshan, central Asia: determined by P and S waveform inversion. J. Geophys. Res. 92, 12629–12648.

Newton, R.C., Perkins, D., 1982. Thermodynamic calibration of geobarometers based on the assemblage garnet – plagioclase – orthopyroxene (clinopyroxene) – quartz. Am. Mineral. 67, 203–222.

Nickel, K.G., Green, D.H., 1985. Empirical geothermobarometry for garnet peridotites and implications for the nature of the lithosphere, kimberlites and diamonds. Earth Planet. Sci. Lett. 73, 158−170.

Norman, M.D., Pearson, N.J., Sharma, A., Griffin, W.L., 1996. Quantitative analysis of trace elements in geological materials by laser ablation ICPMS: instrumental operating conditions and calibration values of NIST glasses. Geostandards Newslett. 20, 247–261.

Pollack, H.N., Chapman, D.S., 1977. On the regional variation of the heat flow, geotherm and lithospheric thickness. Tectonophysics 38, 279–296.

Pouchou, J.L., Pichoir, F., 1984. A new model for quantitative X-ray microanalysis Part 1: application to the analysis of homogeneous samples. Recherche Aerospatiale 5, 13–38.

Powell, R., Powell, M., 1977. Geothermometry and oxygen barometry using coexisting iron-titanium oxides: a reappraisal. Mineral. Mag. 41, 257–263.

Poupinet, G., Avouac, J.Ph, Jiang, M., Wei, S., Kissling, E., Herquel, G., Guibert, J., Paul, A., Wittlinger, G., Su, H., Thomas, J.C., 2002. Interacontinental subduction and Paleozoic inheritance of the lithosphere suggested by a teleseismic experiment across the Chinese Tianshan. Terra Nova 14, 18–24.

Rudnick, R.L., 1995. Making continental crust. Nature 378, 571–578.

Ryabchibov, I.D., Kovalenko, V.I., Ionov, D.A., Solovova, I.P., 1983. Thermodynamic parameters of mineral equilibrium in garnet-spinel lherzolites from Mongolia. Geokhimia 7, 967–980.

Shi, Y.S., Lu, H.F., Jia, D., Cai, D.S., Wu, S.M., Chen, C.M., Howell, D.G., Valin, Z.C., 1994. Paleozoic plate-tectonic evolution of the Tarim and western Tianshan regions, western China. Int. Geol. Rev. 36, 1058–1066.

Sobel, E., Arnaud, R.N., 2000. Cretaceous-Paleogene basaltic rocks of the Tuoyun basin NW China and the Kyrgyz Tianshan: the trace of a small plume. Lithos 50, 191–215.

Spencer, K.J., Lindsley, D.H., 1981. A solution model for coexisting iron-titanium oxides. Am. Mineral. 66, 1189–1201.

Stosch, H.G., Ionov, D.A., Puchtel, I.S., Galer, S.J.G., Sharpouri, A., 1995. Lower crustal xenoliths from Mongolia and their bearing on the nature of the deep crust beneath central Asia. Lithos 36, 227–242.

Stosch, H.G., Schmucker, A., Reys, C., 1989. The nature and geological history of the deep crust under the Eifel Germany. Terra Nova 4, 53–62.

Wang, Y.B., Wang, Y., Liu, X., Fu, D.R., Xiao, X.C., 2000. Geochemical characteristics and genesis of late Cretaceous to Paleoene basalts in Tuoyun basin, south Tianshan Mountain. Acta Petrologica Mineral. 19, 131–139 (in Chinese).

Wells, P.R.A., 1977. Pyroxene thermometry in simple and complex systems. Contrib. Mineral. Petrol. 62, 129–139.

Windley, B.F., Allen, M.B., Zhang, C., Zhao, Z.Y., Wang, G.R., 1990. Paleozoic accretion and Cenozoic re-deformation of the Chinese Tianshan range, Central Asia. Geology 18, 128–131.

Xiao, X.C., Tang, Y.Q., Feng, Y.M., 1992. Tectonics of North Xinjiang and its Adjacent Region. Geological Publishing House, Beijing, pp. 55–60 (in Chinese).

Xu, Y., Liu, F.T., Liu, J.H., 1998. Upper mantle structure in the Tianshan and its geodynamic role to crustal tectonic movement. Seismol. Geol. 20, 405–412 (in Chinese).

Xu, Y., Liu, F.T., Liu, J.H., Sun, R.M., 2000. Crustal structure and tectonic setting of the Tianshan seismic zone, Xinjiang China. Acta Geophys. Sinica 43, 184–193 (in Chinese).

Zheng, J.P., Griffin, W.L., O'Reilly, S.Y., Zhang, M., Pearson, N.J., 2005. Lithospheric mantle beneath the Tianshan area, NW China. Contrib. Mineral. Petrol. (in review).

Zheng, J.P., Griffin, W.L., O'Reilly, S.Y., Lu, F.X., Wang, C.Y., Zhang, M., Wang, F.Z., Li, H.M., 2004. 3.6 Ga lower crust in central China: new evidence on the assembly of the North China Craton. Geology 32, 229–232.

Zheng, J.P., Lu, F.X., O'Reilly, S.Y., Luo, Z.H., 2001. Trace element of Tuoyun mantle clinopyroxene: Implication for the deep processes of lithospheric mantle beneath the southwest Tianshan, west China. Chin. Sci. Bull. 46, 1206–1211.